geosciences

MDPI

Article

Geochemistry and Petrogenesis of Permo–Triassic Silicic Volcanic Rocks from the Circum-Rhodope Belt in the Vardar/Axios Zone, Northern Greece: An Example of a Post-Collision Extensional Tectonic Setting in the Tethyan Realm

Argyro Asvesta

Department of Mineral Resources Engineering, Faculty of Engineering, University of Western Macedonia, 50100 Kozani, Greece; aasvesta@uowm.gr

Abstract: The western side of the Vertiskos Unit crystalline basement in northern Greece is fringed by a Permo–Triassic low-grade metamorphic volcano-sedimentary complex that belongs to the Circum-Rhodope Belt (CRB), which is an important part of the Vardar/Axios oceanic suture zone. The silicic volcanic rocks from the CRB are mainly rhyolitic to rhyodacitic lavas with aphyric and porphyritic textures as well as pyroclastic deposits. In this study, geochemical data obtained with X-ray fluorescence (XRF) for the CRB silicic volcanic rocks are reported and discussed to constrain their petrogenesis and tectonic setting. The rocks are peraluminous and show enrichment in K, Rb, Th, Zr, Y, and Pb while being depleted in Ba, Sr, Nb, P, and Ti, and they have Zr + Nb + Y + Ce > 350 ppm, which are characteristic features of anorogenic A-type granites. They have a Y/Nb ratio > 1.2 and belong to A2-subtype granitoids, implying crust-derived magma in a post-collisional tectonic setting. The high Rb/Sr ratio (3.45–39.14), the low molar CaO/(MgO + FeO_t) ratio, and the CaO/Na_2O ratio (<0.5), which they display, indicate that metapelites are the magma sources. Their low Al_2O_3/TiO_2 ratio (<100), consistent with their high zircon saturation temperatures (average T_{Zr} = 886 °C), and their low Pb/Ba ratio (average 0.06) reveal that they were generated by biotite dehydration melting. The increased Rb/Sr ratio relative to that of presumable parental metapelites of the Vertiskos Unit, coupled with their low Sr/Y ratio (0.12–1.08), reflects plagioclase and little or no garnet in the source residue, indicating magma derivation at low pressures of 0.4–0.8 GPa that correspond to a depth of ~15–30 km. The nearby tholeiitic basalts and dolerites, interstratified with the Triassic pelagic sediments, indicate bimodal volcanism in the region. They also support a model involving an upwelling asthenosphere that underplated the Vertiskos Unit basement, supplying the heat required for crustal melting at low pressures. The Permo–Triassic magmatism marks the transition from an orogenic to an anorogenic environment during the initial stage of continental breakup of the Variscan basement in a post-collision extensional tectonic framework, leading to the formation of the nascent Mesozoic Neo-Tethyan Maliac–Vardar Ocean. This apparently reveals that the Variscan continental collision between the Gondwana-derived Vertiskos and Pelagonian terranes must have been completed by at least the earliest Late Permian.

Keywords: A2-subtype rhyolites; post-collisional extension; crust-derived magma; LP–HT melting conditions; basaltic underplating; Permo–Triassic; Circum-Rhodope Belt; Maliac–Vardar Ocean

Academic Editor: Jaime Cuevas Rodríguez

Received: 15 December 2024
Revised: 5 January 2025
Accepted: 19 January 2025
Published: 2 February 2025

Citation: Asvesta, A. Geochemistry and Petrogenesis of Permo–Triassic Silicic Volcanic Rocks from the Circum-Rhodope Belt in the Vardar/Axios Zone, Northern Greece: An Example of a Post-Collision Extensional Tectonic Setting in the Tethyan Realm. *Geosciences* **2025**, *15*, 48. https://doi.org/10.3390/geosciences15020048

1. Introduction

The Hellenic orogen, known as Hellenides [1], is an integral part of the Alpine–Himalayan collision belt. The Late Permian–Early Triassic was a significant period for the tectonic evolution of the eastern Mediterranean region and the Hellenides. During this period, the southern foreland of the European Variscan orogenic belt (the western peri-Tethys region) underwent a widespread extension associated with the northward rollback of the subducted lithospheric slab of Palaeo-Tethys. The breakup of the supercontinent Pangea started, and a net of continental rifts announced the birth of the Neo-Tethyan oceanic realm. This resulted in the dispersion of Variscan continental fragments and triggered the opening of several Mesozoic "rift" or "back-arc" marginal basins (e.g., Meliata, Maliac) that later coalesced to create the Mesozoic Neo-Tethyan Vardar Ocean (e.g., [2–7]). The Mesozoic Neo-Tethyan Ocean(s) in Greece partly closed during the Mid- to Late Jurassic, leading to ophiolite emplacement (the Vardar/Axios suture zone and Pindos ophiolites) and was ultimately eliminated during the Early Tertiary Alpine collision (e.g., [8–14]). Pre-Alpine basement complexes representing parts of the Variscan continental fragments occur, and they are integrated into the Alpine Hellenic orogen, i.e., the Rhodope Massif, the Serbo-Macedonian Massif, and the Pelagonian Zone.

The early stages of the opening of the Mesozoic Neo-Tethyan basins were characterized by sedimentation (continental clastic and carbonate sediments) in grabens and bimodal magmatism (e.g., in Hellenides [15–20], Dinarides [21], Carpatho-Balkanides [22–24], Pontides [25], and Anatolides [26]). A-type granites and/or bimodal volcanic rocks (A-type rhyolites and tholeiitic basalts) are diagnostic rock types related to extensional environments, specifically associated with anorogenic within-plate (A1-subtype granitoids) and/or post-collision (A2-subtype granitoids) tectonic settings (e.g., [27–36]). A1-subtype granitic magmatism typically has a long duration and is generally separated from compressional tectonic events by 50 to 100 million years or more. In contrast, A2-subtype granitic magmatism is generally short-lived and is usually formed 10 to 20 million years after compressional tectonism and precedes continental fragmentation after periods of collision [29].

In northern Greece, the Vertiskos Unit crystalline basement of the Serbo-Macedonian Massif (SMM) was intruded by Mesozoic A-type leucocratic granites named "Arnea" and "Kerkini" granitic suites. This magmatism was initially considered Middle Triassic anorogenic and was associated with the rift that led to the opening of the Neo-Tethyan Vardar-Meliata Ocean [17,20,37–40]. However, later geochemical and geochronological data of the Arnea and Kerkini granites indicated an A2-subtype magmatism generated in a post-collision extensional tectonic environment during the initial stage of continental rifting at the Permian–Triassic boundary [18,41].

Spatially and temporally associated with the Arnea and Kerkini granitic suites are the silicic volcanic rocks (mostly meta-rhyolites) of the Silicic Volcano-Sedimentary (SVS) succession, which is part of the Permo–Triassic volcano-sedimentary complex that belongs to the Circum-Rhodope Belt (CRB) [18,19]. Minor meta-basic volcanic rocks of the Late Ladinian to Late Triassic age [42] exist in the CRB, indicating that the silicic volcanism was followed by basic volcanism, resulting in a bimodal volcanic sequence [12,16,19,42–47]. The facies architecture of the SVS succession reveals that the volcanic activity evolved in a subaerial–coastal depositional environment that progressively changed to a shallow submarine setting and records the Permo–Triassic stratigraphy of the western continental margin of the Vertiskos Unit crystalline basement [19]. According to Asvesta and Dimitriadis, the SVS succession was formed during the early stages of rifting, which led to the formation of the main oceanic basin of the Vardar/Axios Zone [19]. Ferrière et al. have the same aspect regarding the Nea Santa series (sandstones, rhyolites, Early Triassic to Ladinian carbonate platform) as the remnants of the "proximal eastern margin" of the Maliac Ocean,

which deepened from east to west [12]. Furthermore, Vergely and Mercier interpret it as the continental margin of the East Peonias subzone of the Vardar/Axios Zone [14].

The geochemistry of the extensive Permo–Triassic silicic and minor basic volcanic rocks (bimodal volcanics) from the CRB, along with that of the Arnea and Kerkini granites, is the key to interpreting the specific extensional tectonic setting in which this magmatism evolved. The present paper, as part of a wider study of the Permo–Triassic volcano-sedimentary complex in the CRB [16,19,43–46,48], focuses on the geochemistry of the silicic volcanic rocks. The aim of this research is to clarify (1) the magma type of these silicic volcanic rocks; (2) their magma source regions and their melting conditions; and (3) their tectonic environment, providing new knowledge of their petrogenesis and geodynamic processes. The geochemical link between the CRB silicic volcanic rocks and the Arnea and Kerkini granites is also investigated. Furthermore, this study aims to shed light on the transitional period between the Variscan and Alpine cycles during the Permo–Triassic, which is a time when the lithospheric thinning marked the opening of the future Maliac–Vardar Ocean.

2. Geological Setting and Local Stratigraphy

The NNW–SSE-directed Vardar/Axios Zone [49,50] belongs to the Internal Hellenides and is located in the region of central Macedonia in northern Greece. North of the Greek frontiers, the zone extends into North Macedonia, while to the south, it continues beneath the Aegean Sea and turns southeastwards. It intervenes between two major Palaeozoic continental fragments, the Pelagonian Zone in the west and the Serbo-Macedonian Massif (SMM) plus Rhodope Massif in the east (Figure 1). The Vardar/Axios Zone is the major oceanic suture zone in Greece, and its ophiolites are the remnants of a Mesozoic Neo-Tethyan oceanic crust (the Almopias Ocean and Peonias back-arc Basin) [9,49,51–57]. Moreover, the Pindos, Vourinos, and Orthris ophiolites are exposed on the west side of the Pelagonian Zone. According to some authors, the Pindos–Vourinos–Orthris ophiolites and the Vardar/Axios suture zone were formed by two Neo-Tethyan oceans that lay on either side of the Pelagonian continental fragment (e.g., [9,58–63]). Another group of scientists claims that there were more than two Neo-Tethyan oceans in Greece (e.g., [10,14,64]). However, many authors believe that all the ophiolites originated from a single ocean situated between the Pelagonian and Serbo-Macedonian fragments with their position on the western Pelagonian side being tectonically explained as having been thrust from east to west (e.g., [12,13,58,65–71]). Ferrière et al. consider that this ocean, known as "the Maliac Ocean," was the major Hellenic Tethyan Ocean represented by the ophiolites [12]. Kilias also suggests that all ophiolites in the Hellenides were derived from a single source: the Neo-Tethyan "Meliata/Maliac–Axios/Vardar Ocean" [13].

The Vertiskos Unit crystalline basement is a Gondwana-derived terrane that covers a major part of SMM in Greece [72–75]. The continuation of the Vertiskos Unit in North Macedonia and Serbia is referred to as "the Lower Complex" and in Bulgaria as "the Ograzhden block" ([76] and references therein). The Vertiskos Unit consists of migmatitic paragneisses and orthogneisses, representing pre-Alpine continental crust, with pegmatite veins. It also contains lenses of amphibolite and serpentinite [72,73,77,78]. It records four metamorphic events: (1) a Variscan ultrahigh pressure event, (2) a Triassic low-pressure (LP) and high-temperature (HT) event, (3) a Late Jurassic–Early Cretaceous moderate high-pressure (HP) event, and (4) a low-pressure (LP) metamorphic event in the Late Cretaceous [73,77–81].

Permian–Mesozoic A-type leucocratic meta-granites, the Arnea and Kerkini Granitic Suites [37], intruded into the Silurian orthogneiss of the Vertiskos Unit. Himmerkus et al. attribute a Triassic age (227–229 Ma) to the Kerkini granite [40], while Christofides et al. and

Poli et al. suggest an age around the Permo–Triassic boundary (247 Ma) [17,18,39]. For the Arnea granite, Kostopoulos et al. propose a Late Triassic age of 215 Ma [82], Himmerkus et al. estimate approximately 228 Ma [40], and Poli et al. report ages of 254 and 244 Ma, also near the Permo–Triassic boundary [18].

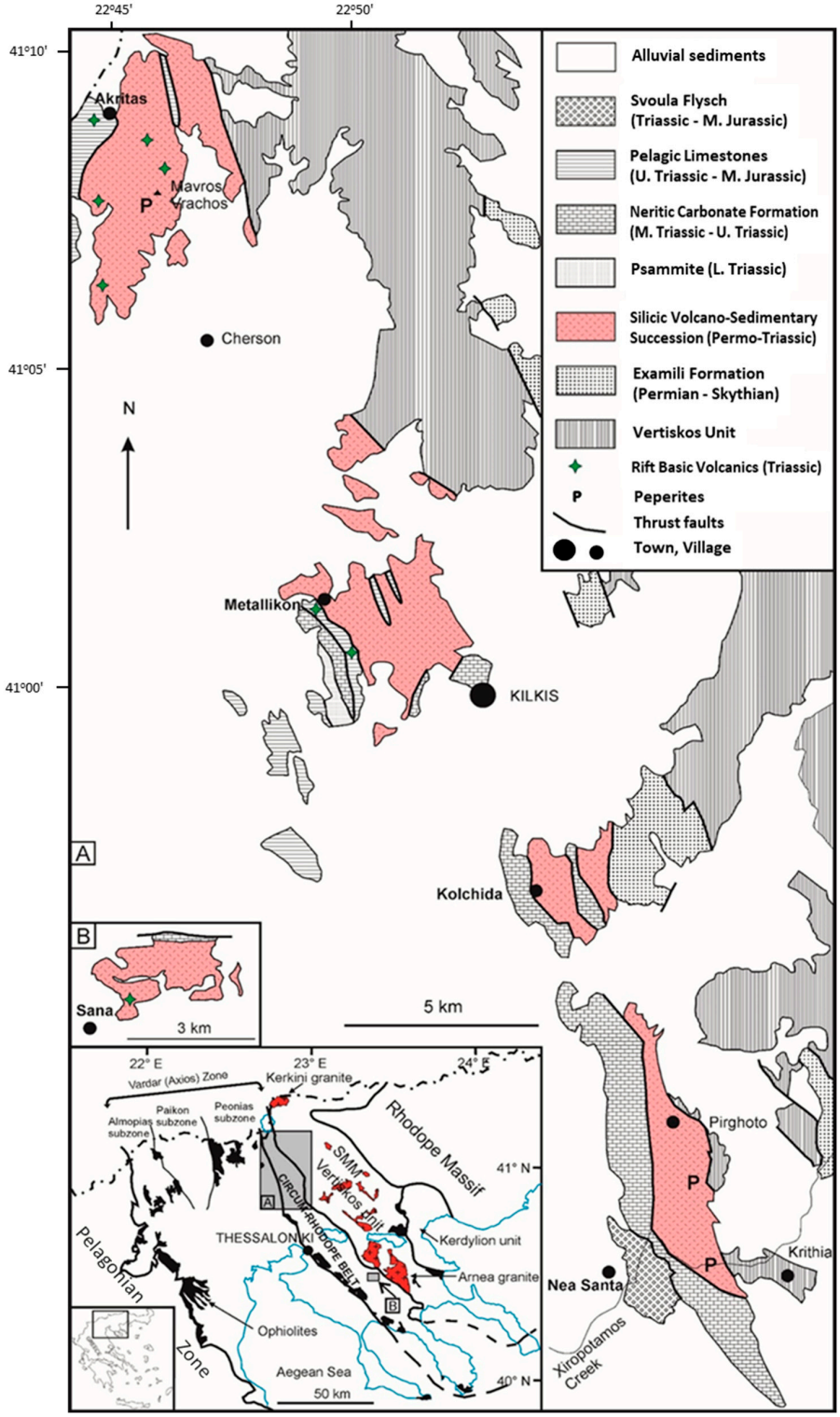

Figure 1. Geological map that illustrates the lithostratigraphic sequence of the Permo–Triassic volcano-sedimentary complex in the Circum-Rhodope Belt. The A and B mapped areas are indicated on the inset map to the left of the figure. From [44], modified after [16,49,83].

The eastern part of the Vardar/Axios Zone, named as "the Peonias subzone" [49], comprises the Circum-Rhodope Belt (CRB) [72,73,84]. In the CRB, a Permo–Triassic volcano-sedimentary complex metamorphosed in the greenschist-facies crops out discontinuously in a NNW–SSE direction, fringing the western part of the Vertiskos Unit, approximately parallel to the Vardar oceanic suture zone (Figure 1). It comprises subaerial to submarine volcanic and sedimentary rocks that are tectonically telescoped, overturned, and deformed, displaying a northeast-dipping cleavage [19]. This is likely the result of two compression events: one in the Late Jurassic, which also caused the greenschist-facies metamorphism, and the other in the Early Tertiary [49,72,73]. Despite the low-grade metamorphism, the original sedimentary and volcanic features of the rocks are well preserved, and the prefix "meta-" is sometimes omitted in the following.

The lithostratigraphic sequence of the Permo–Triassic volcano-sedimentary complex reveals four units, formations, and successions. The contacts between them are tectonic, but they are generally thought to represent tectonized original stratigraphic boundaries [16,19,42,43,47,49,73,83–86]. The sequence, from bottom to top, is as follows (Figure 2):

(a) The Examili Formation;
(b) The Silicic Volcano-Sedimentary (SVS) succession [19], also referred to as "the Volcanosedimentary Series" [49,73,87] and "the Pirghoto Formation" of the Nea Santa Unit [42,85];
(c) The neritic carbonate sedimentary facies of the Svoula Formation; and
(d) The pelagic sedimentary facies of the Metallikon and Megali Sterna Units with interstratified meta-basic rocks.

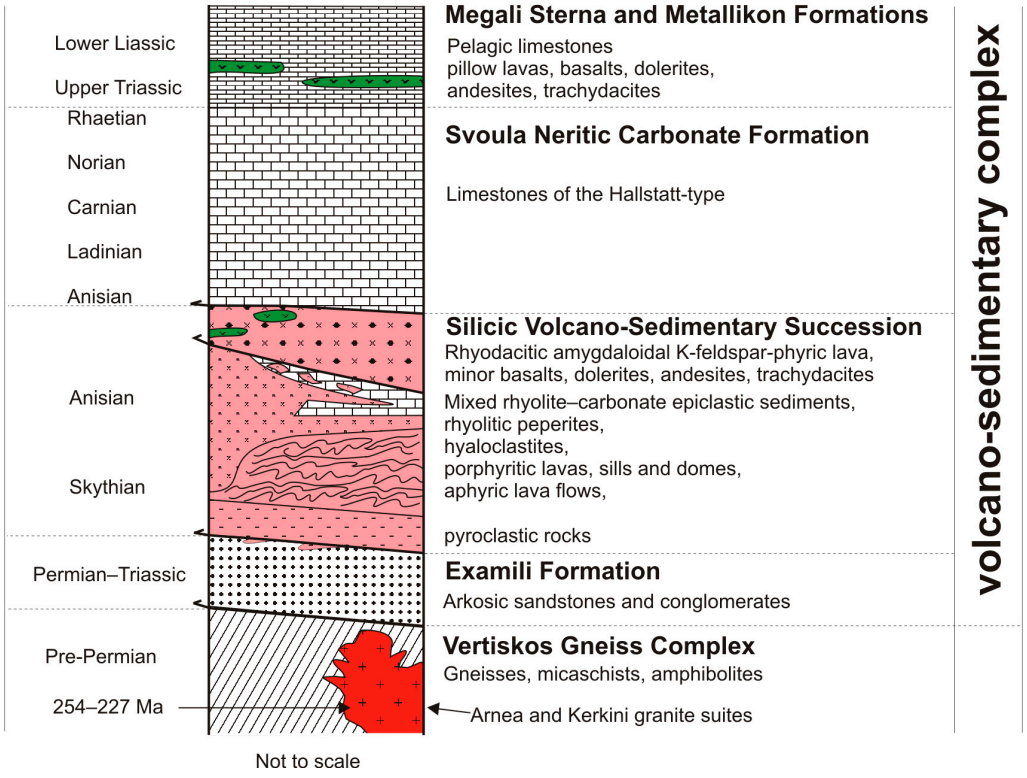

Figure 2. Synthetic tectonostratigraphic columnar section of the Permo–Triassic volcano-sedimentary complex from the Circum-Rhodope Belt in northern Greece. From [44], modified after [19,49,83,85].

(a) The Examili Formation is composed of terrigenous deposits that are poorly sorted, immature, unfossiliferous, meta-arkoses, meta-psammites, and conglomerates. It is

generally accepted that it is Permian–Scythian in age [73,86,88] because of the time constraints imposed by the stratigraphically overlying Silicic Volcano-Sedimentary (SVS) succession. It is interpreted as alluvial fan deposits that accumulated at the base of normal faults formed in the Vertiskos Unit basement during the initial stages of an extensional tectonic basin. The lithology of its clasts indicates the Vertiskos Unit as the likely source provenance [16,43,85,86]. It is the first formation that was deposited on the future western margin of the Vertiskos terrane or, according to Ferrière et al. [12], on the eastern proximal margin of the Maliac Ocean.

(b) The Silicic Volcano-Sedimentary (SVS) succession consists of silicic volcanic rocks (mostly rhyolites to rhyodacites) and neritic carbonate sediments. It is up to 3000 m in thickness (Volcanosedimentary Series; [87]) and comprised two parts [19]. The lower part consists of pyroclastic rocks and porphyritic and aphyric flow-banded lavas emplaced in a subaerial–coastal environment. The upper part consists of quartz–feldspar–phyric lavas and domes, hyaloclastites, sills interbedded with neritic carbonate sediments, peperites, and epiclastic sedimentary rocks with rhyolitic and carbonate clasts, suggesting a submarine depositional environment.

In addition, the SVS succession exposed in the Akritas and Metallikon areas comprises rhyodacitic, amygdaloidal, K-feldspar-phyric lava [16]. Some lava samples exhibit microtextures indicative of magma mixing or contain mafic microgranular enclaves [45]. Small exposures of the same lava are also present further south near the village of Sana. Rhyolitic dykes intruding the gneiss of the Vertiskos Unit, near the villages of Nea Santa [16,19] and Zagliveri [86], were likely feeder dykes for the volcanic rocks.

According to the findings obtained by Ferrière and Stais [42], the fauna in the overlying and interbedded limestones (foraminifera "*Rectocornuspira Kalhori*") reveal that the SVS succession is Early to Middle Triassic in age and probably reaches Permian age in its lower part. Furthermore, U–Pb zircon dating in a rhyolite yielded an age of circa 240 Ma (R. Frei cited in [82]).

(c) The neritic carbonate sedimentary facies of the Svoula Formation [73,86] is mostly composed of thick, recrystallized, and partly dolomitized and silicified fossiliferous neritic limestones. It is dated to the Upper Scythian–Upper Triassic based on fossil findings, including crinoids, corals, echinoderms, and foraminifera [16,42,47,49,73,86].

(d) The Upper Ladinian–Rhaetian pelagic sedimentary facies of the Metallikon and Megali Sterna Units overlay the neritic carbonates. They consist of a carbonate conglomerate and alternating platy, micritic limestone layers with nodules, gray in color, and mudstone, pelagic chert, and carbonate sediments. In the area near Metallikon village (Figures 1 and 2), this pelagic facies contains small interstratifications of altered, low-grade metamorphic dolerite and basalt [16,19,42–44,47]. The age of these meta-basic rocks is probably Mid–Late Triassic (Late Ladinian–Rhaetian), as is indicated by the presence of foraminifera in the intercalated sedimentary units and Carnian conodonts in the overlying carbonate sediments [42,47]. In the area near Akritas village (Figures 1 and 2), intercalations of the same basalt and dolerite, in addition to minor andesite and trachydacite, occur in the pelagic lime-marl-layered sedimentary facies of the Megali Sterna Unit [16,43]. Furthermore, the same meta-basic rocks intervene within the rhyodacitic amygdaloidal lava near Akritas village (Figures 1 and 2). The Akritas–Metallikon meta-basic rocks, named by Asvesta and Dimitriadis [44] as "the Triassic Rift Basic Volcanics" or, according to Ferrière et al. [12], as "the East Maliac Margin Triassic Basic Volcanics," show mid-ocean ridge basalt (MORB) to within-plate basalt (WPB) affinity [16,43,44,46], and their presence implies that the Triassic volcanism was bimodal [16,19,43–46].

3. Petrography

The CRB silicic volcanic rocks are represented by porphyritic and aphyric rhyolitic to rhyodacitic lavas and pyroclastic rocks, which were altered and metamorphosed to greenschist facies [19].

The porphyritic rhyolites, mostly green in color, contain quartz and K-feldspar phenocrysts (about 30%) as well as a few albite and zircon crystals. The quartz phenocrysts are subhedral, and some of them display corrosion embayment. The K-feldspar phenocrysts are perthitic microcline, altered to kaolinite and sericite, and rarely corroded. Quartz and sericite are the alteration products of the previous glassy groundmass (Figure 3a,b).

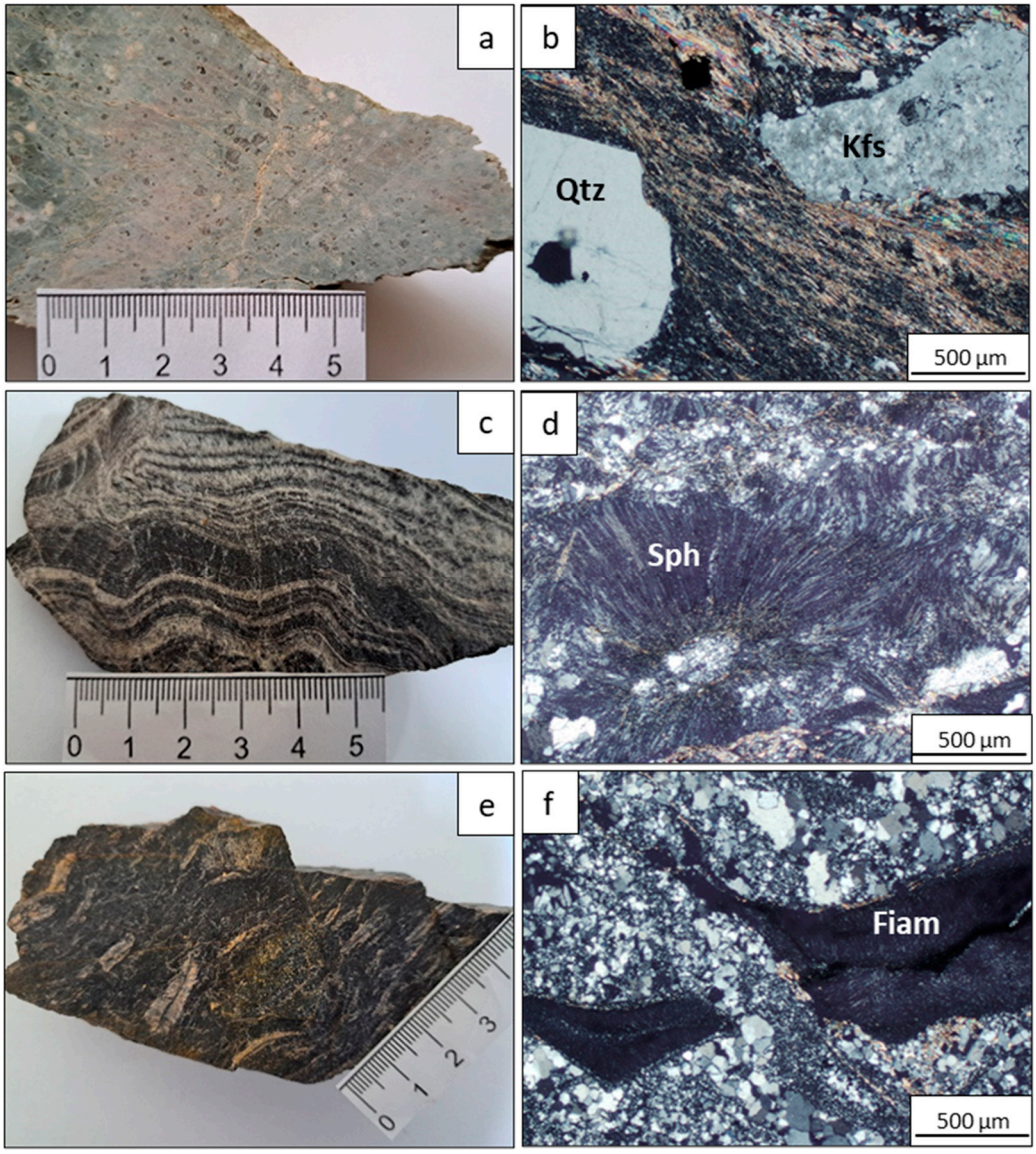

Figure 3. Representative hand specimen photos and photomicrographs of thin sections (crossed nicols) of the CRB silicic volcanic rocks: (**a**,**b**) porphyritic rhyolite; (**c**,**d**) aphyric lava; (**e**,**f**) pyroclastic rock. Qtz: quartz, Kfs: K-feldspar, Sph: spherulite, Fiam: fiamme. See also text for more explanations.

The aphyric lavas are characterized by flow banding with alternating light- and dark-colored bands, such as black lavas with gray and white bands, gray lavas with black, green, and red bands, and pale purple lavas with dark purple bands. They also present a variety of flow folds. Under the petrographic microscope, it is obvious that the flow banding is defined by alternating layers of vesicular pumice and obsidian. The vesicles are infilled

with vapor-phase minerals, mostly quartz. Rarely, some euhedral crystals of barite are present as infills in pumice vesicles. Moreover, quartz-feldspar microspherulites have grown around the margins of vesicles, and sericite has formed as a result of devitrification, hydrothermal alteration, and low-grade metamorphism (Figure 3c,d).

The pyroclastic rocks show a variety of colors and consist of well-preserved, dense, or pumiceous rhyolitic fiamme, millimeter- to centimeter-sized, that are embedded in a silicified and recrystallized matrix. The fiamme are blocky or lenticular in shape and show cuspate, or ragged edges. Under the petrographic microscope, the cuspate fiamme reveals fine axiolitic devitrification, i.e., acicular crystals growing inward from the walls of the fiamme, which is known as pectinate texture. Spherulitic texture is also present in some fiamme. Fragments of K-feldspar crystals occur sparsely, whereas quartz crystals are rare. The matrix is composed mostly of fine-grained quartz and rarely of sericite, products of devitrification and recrystallization of previous fine vitric ash and glass shards (Figure 3e,f).

4. Sampling and Analytical Methods

The CRB silicic volcanic rocks are grouped into five distinct outcrops, each named after a nearby village: Akritas, Metallikon, Nea Santa, Kolchida, and Sana (Figure 1). Sixty-three (63) of the least-altered representative rock samples were petrographically selected for whole-rock chemical analysis. Of these, eleven (11) samples are from Akritas, nineteen (19) from Metallikon, seventeen (17) from Kolchida, eight (8) from Nea Santa, and eight (8) from the Sana area.

The analyses for major oxides and trace elements were performed on a Philips PW 1450/20 X-ray fluorescence (XRF) spectrometer at the Grant Institute, School of Geosciences, University of Edinburgh, using standard operating procedures. The concentrations of major elements were determined using fused glass discs, and for trace elements, using pressed powder pellets. The bulk geochemical data of the investigated CRB silicic volcanic rocks, their normative mineralogical compositions (calculated CIPW norms), their zircon saturation temperature estimates (T_{Zr}), and some significant elemental ratios are presented in Table S1 (Supplementary Materials; Files: Akritas, Metallikon, Nea Santa, Kolchida, and Sana).

5. Results

The obtained geochemical data indicate that some of the analyzed samples are rich in SiO_2, K_2O, and Al_2O_3, which is likely due in part to silicification, hydrothermal alteration, and metamorphism. Given the effects of alteration and metamorphic processes on element remobilization, petrogenetic and tectono-magmatic interpretations must be based on relatively immobile elements. These are mainly the incompatible high-field strength elements (HFSEs) such as Zr, Nb, Y, Ti, and P [89,90]. The immobile element ratios can provide relatively reliable information on primary geochemistry and petrogenetic characteristics.

5.1. Petrochemical Classification

Winchester and Floyd [91] used the Zr/TiO_2 ratio as an index of differentiation and the Nb/Y ratio as an index of alkalinity to classify volcanic rocks and distinguish between magma series (alkaline—subalkaline). The CRB silicic volcanic rocks are classified mainly as rhyolites, rhyodacites, and partly as dacites, on the Zr/TiO_2 vs. Nb/Y classification diagram (Figure 4). A group of rhyolite samples from the Metallikon area is highly differentiated, as indicated by their relatively high Zr/TiO_2 ratio. The low Nb/Y ratio (<0.67) of the silicic magma series indicates its subalkaline affinity. Moreover, in the AFM ternary diagram of Irvine and Baragar [92], a calc-alkaline magmatic affinity is attributed to the CRB silicic volcanic rocks (Figure 5a).

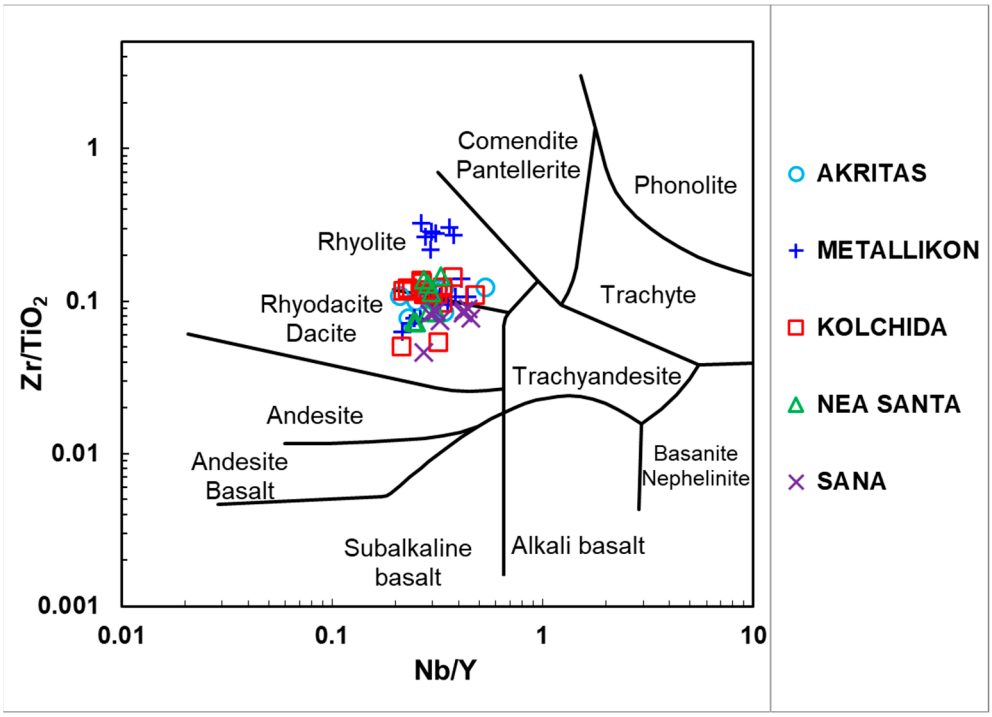

Figure 4. Plot for the CRB silicic volcanic rocks exposed at the Akritas, Metallikon, Nea Santa, Kolchida, and Sana areas on the classification diagram Zr/TiO_2 vs. Nb/Y (after [91]).

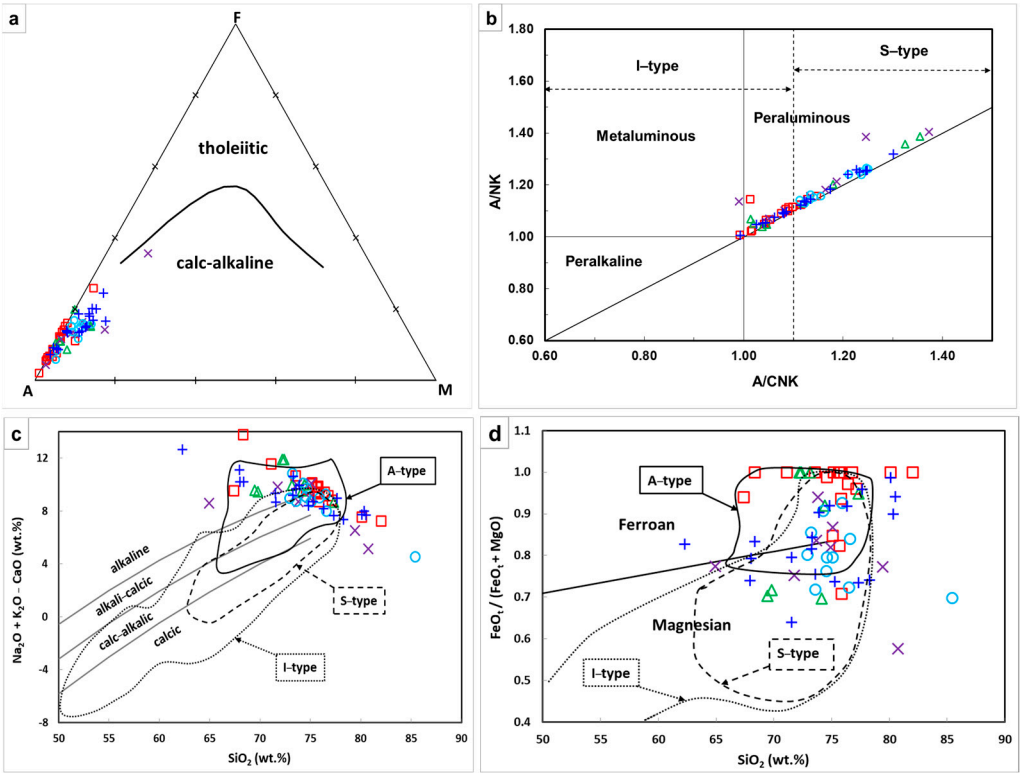

Figure 5. Plot of the CRB silicic volcanic rocks on (**a**) AFM diagram showing the distinction between tholeiitic and calc-alkaline suites [92], (**b**) A/CNK vs. A/NK diagram (fields after [93]), (**c**) $Na_2O + K_2O - CaO$ (MALI, i.e., modified alkali lime index) vs. SiO_2 [94], (**d**) $FeO_t/(FeO_t + MgO)$ vs. SiO_2 [94]; $FeO_t = Fe_2O_3 \times 0.8998\ Fe_2O_3$. Symbols are as in Figure 4.

In terms of alumina saturation index and molecular $Al_2O_3/(Na_2O + K_2O + CaO)$, the CRB silicic volcanic rocks are exclusively peraluminous (ASI and A/CNK > 1.0), being

corundum-normative (0–4.28%; average 1.52%) (Table S1, Figure 5b). Many of them possess an A/CNK ratio ≥ 1.1 and can be characterized as strongly peraluminous (SP) according to Sylvester [95]. In the $Na_2O + K_2O - CaO$ (MALI, i.e., modified alkali lime index) and the $FeO_t/(FeO_t + MgO)$ vs. SiO_2 diagrams of Frost et al. [94], the samples plot on the peraluminous leucogranite field, or A-type granites field, as they span all the range of granitoid compositions from magnesian to ferroan and from calcic to alkaline (Figure 5c,d).

5.2. Major Oxides

The CRB silicic volcanic rocks are enriched in alkalis, with the $K_2O + Na_2O$ contents ranging from 4.63 to 13.83 wt.% (average 9.40 wt.%), and K-rich, with a K_2O/Na_2O ratio higher than 1. They exhibit high Al_2O_3 (7.51 to 17.42 wt.%; average 12.52 wt.%) and Fe_2O_3 (0.51 to 6.73 wt.%; average 1.72 wt.%) contents. They are characterized by low MgO (0.00 to 1.77 wt.%; average 0.37 wt.%), CaO (0.01 to 0.88 wt.%; average 0.12 wt.%), TiO_2 (0.03 to 0.82 wt.%; average 0.26 wt.%), P_2O_5 (average 0.05 wt.%), and MnO (average 0.02 wt.%) contents (Table S1).

Using SiO_2 as an index of fractionation, there is a distinct decreasing trend in the major element oxides (Figure 6). Al_2O_3, Fe_2O_3, MgO, and total alkalis ($K_2O + Na_2O$) exhibit a complete negative correlation with increasing silica content, while TiO_2 and P_2O_5 exhibit a decreasing trend with increasing SiO_2 content up to approximately 68 wt.%, after which their concentrations remain relatively constant. The rock samples with low SiO_2 contents (<68 wt.%), classified as dacites, present a scattering of data points on Harker variation diagrams. Despite this scatter, all the general trends of the major oxides are in accordance with a fractional crystallization model.

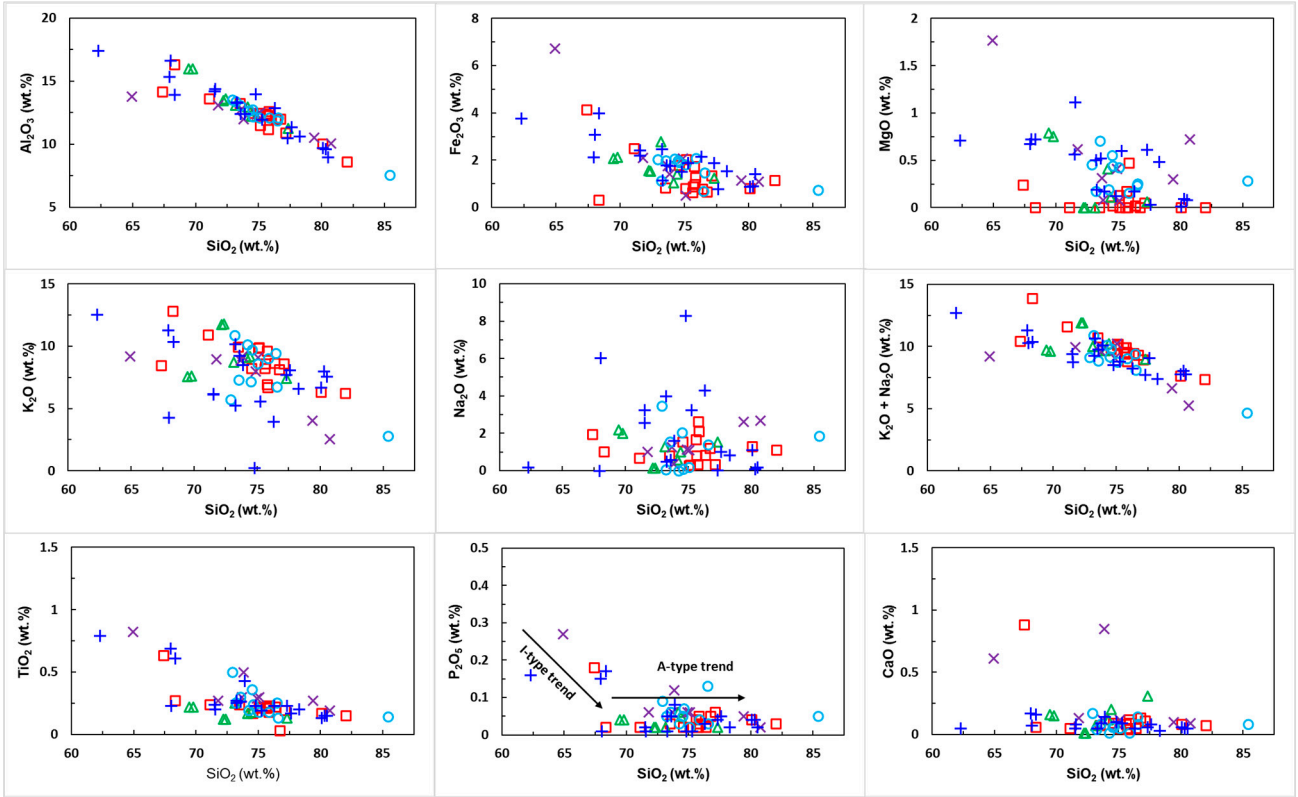

Figure 6. Harker variation diagrams for the CRB silicic volcanic rocks for major element oxides (wt.%). Fe_2O_3 refers to the total Fe_2O_3. I- and A-type trends are after [96]. Symbols are as in Figure 4.

5.3. Trace Elements

The CRB silicic volcanic rocks have relatively low contents of compatible trace elements (Ni average = 7; Cr average = 4; Sc average = 4). In Figure 7, the contents of some trace elements of the rocks against SiO_2 are shown. There is a general decreasing trend for incompatible trace elements (e.g., Zr, Nb, Y, La, Th, Nd, Rb).

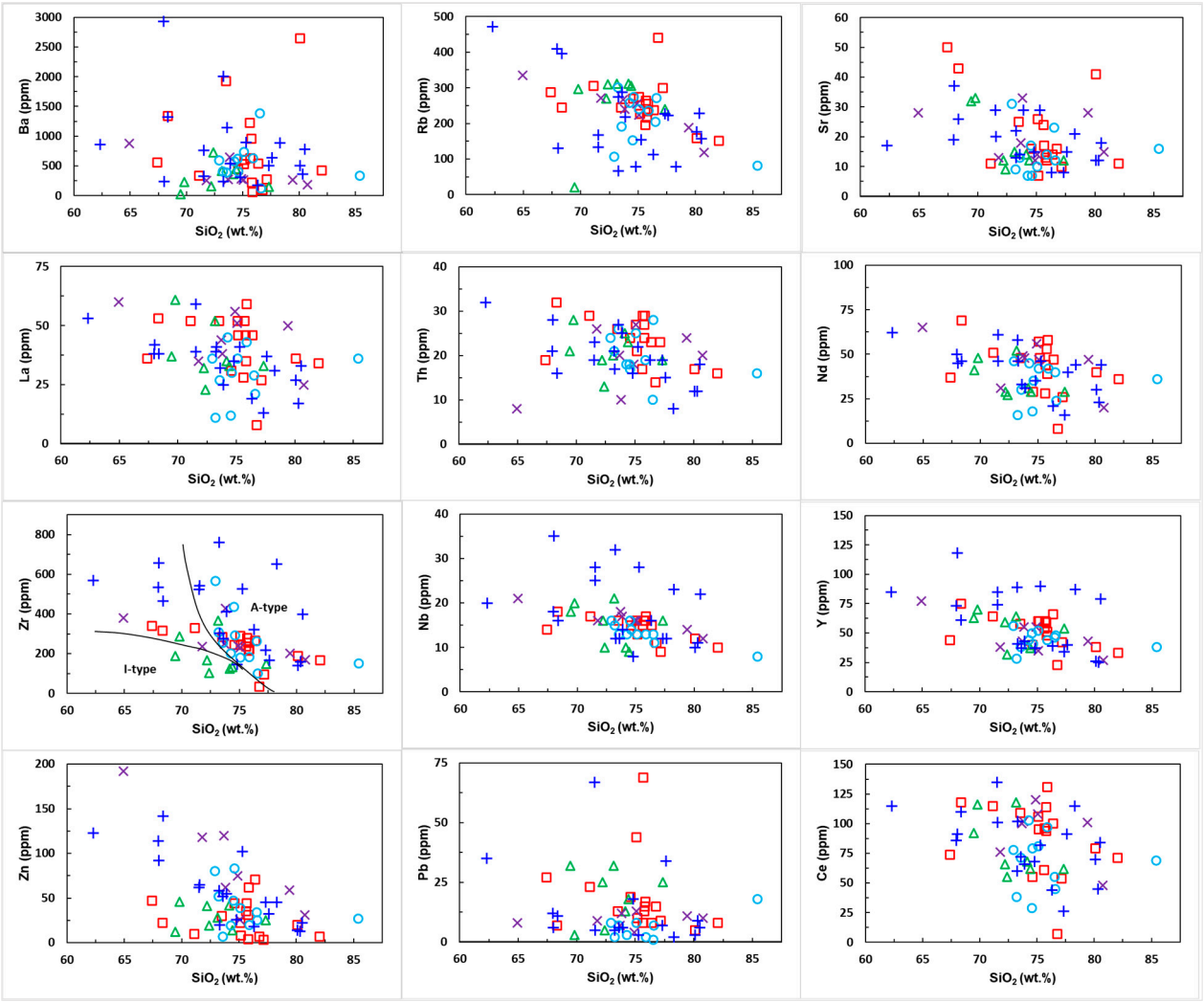

Figure 7. Harker variation diagrams for some trace elements (ppm) of the CRB silicic volcanic rocks. I- and A-type fields are after [96,97]. Symbols are as in Figure 4.

The rocks are characterized by low Sr contents (<50 ppm), low Sr/Y ratio (0.12–1.14; average = 0.37), and high Rb/Sr ratio (3.45–39.14; average = 15.8) as well as Y/Nb ratio > 1.2 (1.87–4.75; average = 3.36) (Table S1). Some significant ratios like Ce/Pb, La/Nb, Ce/Nb, Rb/Ba, Rb/Y, Rb/Nb, Th/Y, Th/Nb, and Pb/Ba (Table S1) are discussed in the next Sections 6.3.1, 6.3.2, 6.3.5 and 6.4.2.

On the primordial mantle normalized [98] multi-element spider diagram (Figure 8), rock samples of all five areas show similar patterns revealing their origin from the same magma. They exhibit a distinctive depletion of large-ion lithophile elements (LILEs) such as Ba, Sr, and high-field strength elements (HFSEs) such as Nb, P, and Ti (negative anomalies), whereas they show an enrichment of Rb, Th, K, and Pb (positive anomalies), which are characteristic features of A-type granites. The pronounced negative anomalies in Ba, Nb, Sr, P, and Ti imply that these peraluminous magmas have undergone fractional crystallization during their magmatic evolution. The anomalies suggest the removal of

feldspar (evidenced by the negative Ba and Sr anomalies), apatite (negative P anomaly), and Fe-Ti oxides (negative Ti anomaly) from the magma. Despite the negative anomalies in Ba, Nb, La, and Ce, the CRB silicic volcanic rocks show an enrichment of these trace elements. High Ba values, mostly in some samples from the Kolchida area (A15, A17, A18, A22; Table S1), are attributed to barite infilling vesicles of pumiceous rhyolitic lavas (microscopic observation).

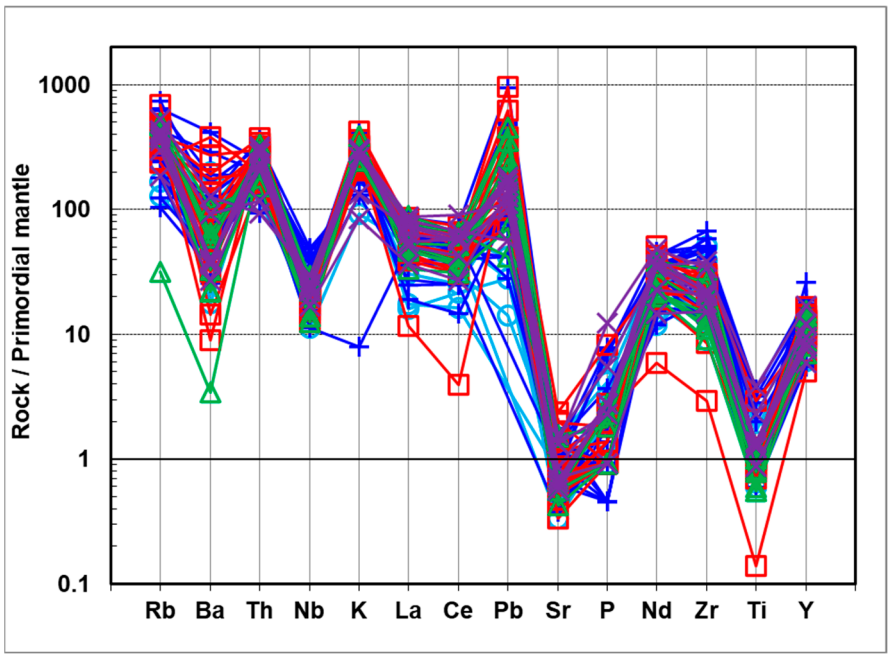

Figure 8. Trace element distribution patterns normalized to the composition of primitive mantle for the CRB silicic volcanic rocks (normalization values are after [98]). Symbols are as in Figure 4.

6. Discussion

6.1. Magma Type

A-type granites were originally characterized by Loiselle and Wones [99] as anorogenic, anhydrous, and reduced. Their identification was based on both tectonic setting and chemical characteristics, whereas the discrimination between I- and S-type granites was strictly based on the different magma sources [100]. A-type granitoids occur in rift zones and within stable regions of continental crust [99].

The major element concentrations of the CRB silicic volcanic rocks indicate that they are peraluminous A-type granitoids. Specifically, the rocks have Al_2O_3 + CaO < 15 wt.%, high SiO_2, high K_2O/Na_2O, FeO_t/MgO and $(Na_2O + K_2O)/CaO$ ratios, high Na_2O + K_2O, and low CaO and MgO (Table S1) [27,35,94,97,99,101,102]. Furthermore, their high CIPW normative corundum (0–4.28%; average 1.52%; Table S1) is consistent with strongly peraluminous S-type granitoids produced by the partial melting of metasediments [103]. In addition, the roughly constant content of P_2O_5 the rocks exhibit (Figure 6) indicates that they are A-type granitoids [96].

The values of some significant trace elements in the CRB silicic volcanic rocks are consistent with the typical geochemical features of A-type granites, such as Zr > 250 ppm, Nb > 20 ppm, Y > 80 ppm, Rb/Sr $\geq$ 3.52, and Zr + Nb + Y + Ce > 350 ppm [27,29,35,101,104,105], along with their low contents in compatible metals Cr, Ni, Sc, and V (Table S1). Moreover, their Zr content decreases toward more felsic compositions (Figure 7), which is similar to the trend observed in A-type magmas derived from quartzofeldspathic sources with Zr saturation [96,97].

Discrimination diagrams for distinguishing A-type granites from the other types like I-, S-, and M-type granites have been proposed by Whalen et al. [27]. In these diagrams, the variation in the major oxide ratios, such as $(K_2O + Na_2O)/CaO$ and (FeO_t/MgO), with (Zr + Nb + Ce + Y) shows that all the samples of the studied silicic volcanic rocks are plotted almost exclusively in the A-type granite field (Figure 9a,b). The Rb/Sr ratio is useful for discrimination between orogenic and anorogenic granites. Granitic suites generated in compressional (orogenic) tectonic settings are characterized by Rb/Sr ratios less than one [106]. In the Rb/Sr vs. K/Rb diagram [107], it is evident that almost all samples of the investigated CRB silicic volcanic rocks (except the sample "A626" from the Nea Santa area) have Rb/Sr ratios greater than one (ranging between 3.45 and 39.14 with an average of 15.8), like A-type granites (Figure 9c).

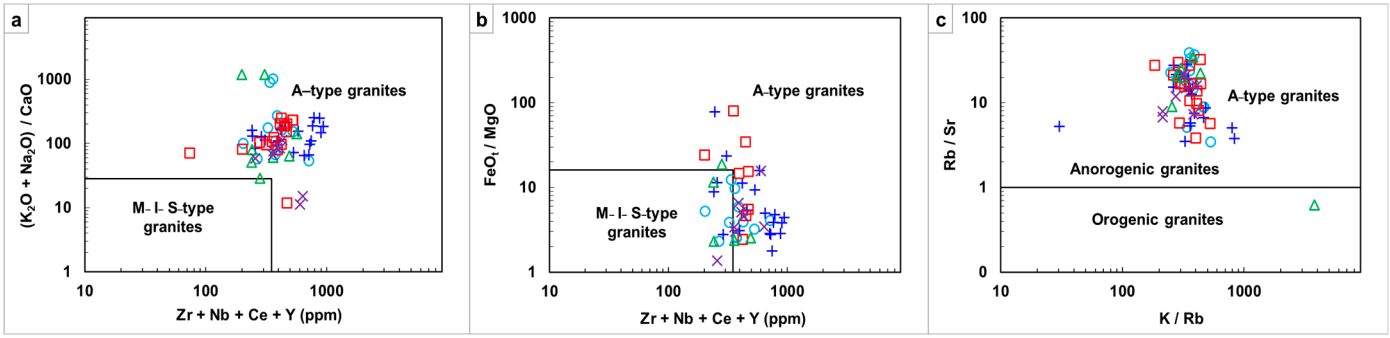

Figure 9. The A-type nature of the CRB silicic volcanic rocks is shown in (**a**) $(K_2O + Na_2O)/CaO$ vs. Zr + Nb + Ce + Y and (**b**) FeO_t/MgO vs. Zr + Nb + Ce + Y discrimination diagrams [27]. (**c**) The K/Rb vs. Rb/Sr diagram [107] reveals that almost all samples of the studied silicic volcanic rocks exhibit Rb/Sr ratios > 1, similar to anorogenic A-type granites, whereas orogenic calc-alkaline granites are characterized by Rb/Sr ratios < 1. Symbols are as in Figure 4.

6.2. Tectonic Setting

As demonstrated above, the CRB silicic volcanic rocks bear the most distinctive geochemical characteristics of A-type granitic magma. Although A-type granitoids were initially thought to evolve in rift zones or stable continental blocks [99], it is generally accepted that they can be formed in both within-plate anorogenic and post-collisional settings [27,29,35,101,108,109]. In the multicationic R1–R2 diagram [110], the CRB silicic volcanic rocks straddle mostly the boundary between anorogenic alkaline and late-orogenic magmatic suites, and some of them plot to the post-orogenic field (the fields are defined by [111]) (Figure 10).

Multi-element spider diagrams normalized to the hypothetical composition of ocean ridge granite (ORG) have been used by Pearce et al. [112] to differentiate between the granite types formed in different tectonic settings. The ORG-normalized patterns of the CRB silicic volcanic rocks from the five outcropping areas are broadly similar with minor variations in the intensity of positive or negative anomalies (Figure 11). They exhibit a negative slope that is attributed to an enrichment of the incompatible elements at the left and progressive depletion toward the more compatible elements on the right side of the spider diagrams. Rb and Th display pronounced positive anomalies and are highly enriched compared to the normalizing values. Ce shows a light positive anomaly. Ba shows a significant negative anomaly except for some pumiceous rhyolite samples (A15, A17, A18, A22) from the Kolchida area, which present microvesicles infilled with barite. The HFS element Nb shows close normalized values with a slight enrichment relative to those of ORG and a small negative anomaly. The HFS element Zr, as well as the Y, also display

close normalized values quite approximate to those of ORG, bringing about a flat change in the pattern.

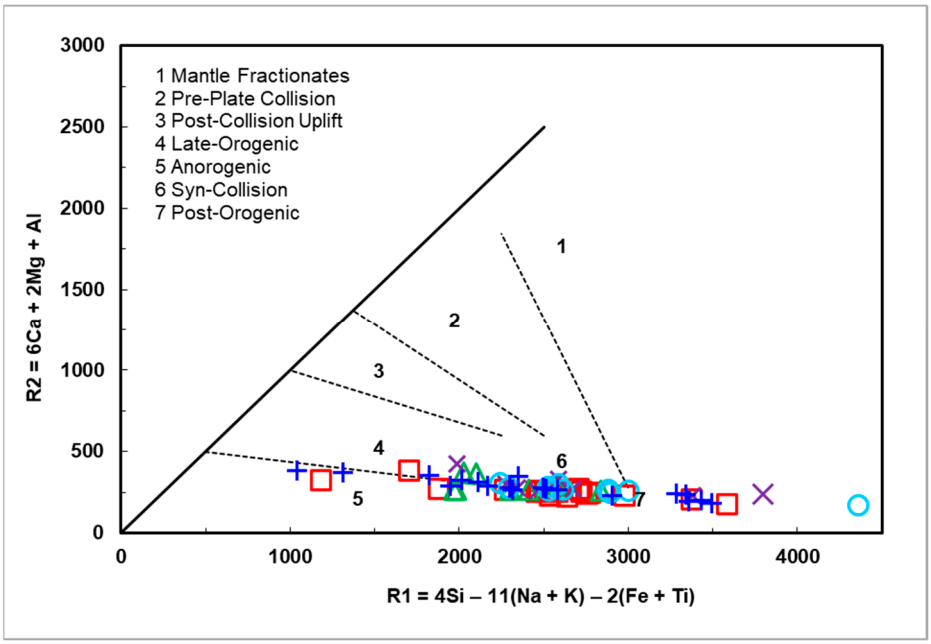

Figure 10. R1–R2 diagram plot [110] of the CRB silicic volcanic rocks. The fields are after [111]. Symbols are as in Figure 4.

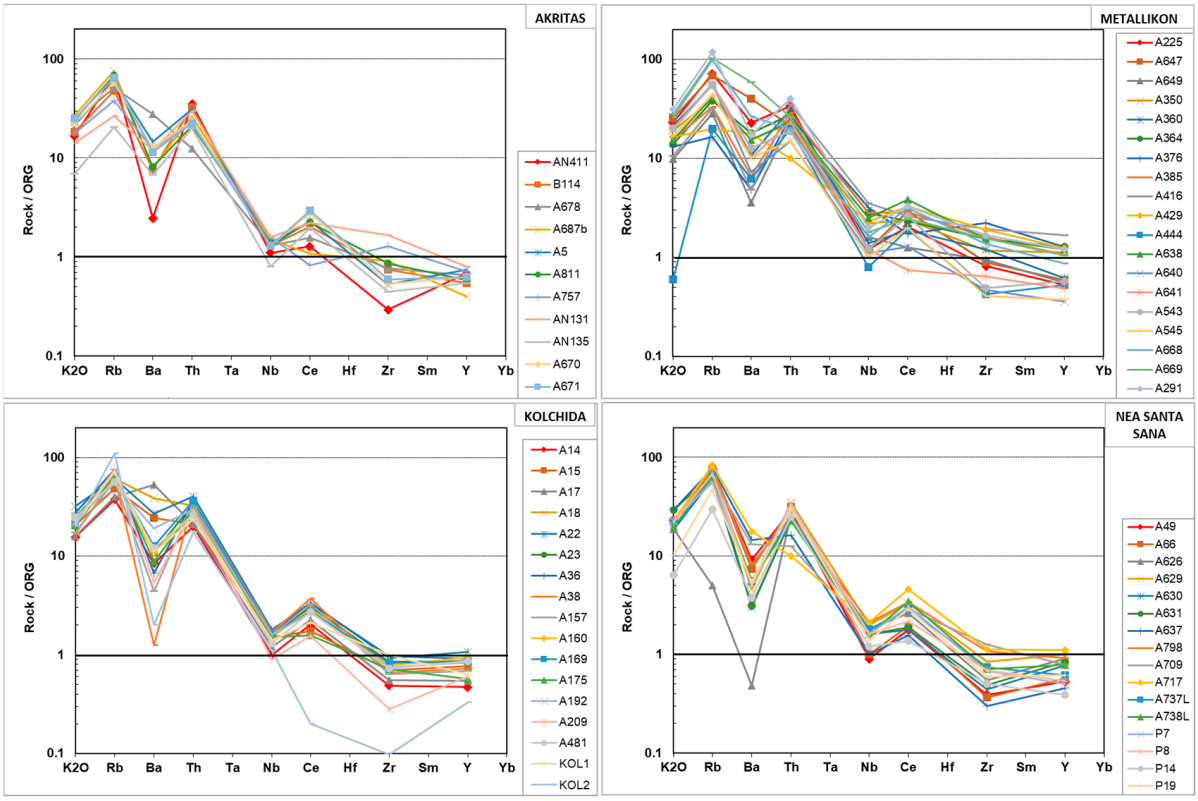

Figure 11. ORG-normalized [112] multi-element spider diagrams of the investigated CRB silicic volcanic rocks.

The normalized element values of the CRB silicic volcanic rocks show the typical characteristic features of the within-plate granites of the attenuated continental lithosphere (Mull and Skaergaard; see Figure 1d in [112]) but also approach the post-collision gran-

ites, particularly those of the Oman granitoids (see Figure 1f in [112]). These tectonic environments are consistent with an extensional tectonic regime. Many samples from the Metallikon area possess higher enrichment levels, especially in the elements Nb, Zr, and Y, revealing more alkalic compositions. This may be due to a possible magma mixing process (topic in other work in progress).

The two tectonic discrimination diagrams for the granites of Pearce et al. [112] reveal that most data points of the CRB silicic volcanic rock samples plot in the field of within-plate granites (Figure 12a,b). Particularly, on the Y vs. Nb diagram (Figure 12a), most of the rocks plot in the overlap zone between within-plate granites (WPGs) from attenuated continental lithosphere and ocean ridge granites (ORGs) from anomalous ridge segments, while fewer samples fall into the volcanic arc and syn-collisional granites field. Moreover, on the binary (Y + Nb) vs. Rb diagram (Figure 12b), most samples fall inside the within-plate granites field, but all the samples are positioned near the triple-junction boundary of the within-plate, volcanic arc, and syn-collisional granites, i.e., the post-collision granites field [113]. On the Rb/Zr vs. SiO_2 diagram [114], they mainly fall into the post-collision granitoid field, except for some samples from the Metallikon and Akritas areas plotting in the volcanic arc field (Figure 12c). This diagram also provides support for an A-type character for the CRB silicic volcanic rocks, as both within-plate and post-collisional granites correspond to A type [27,29].

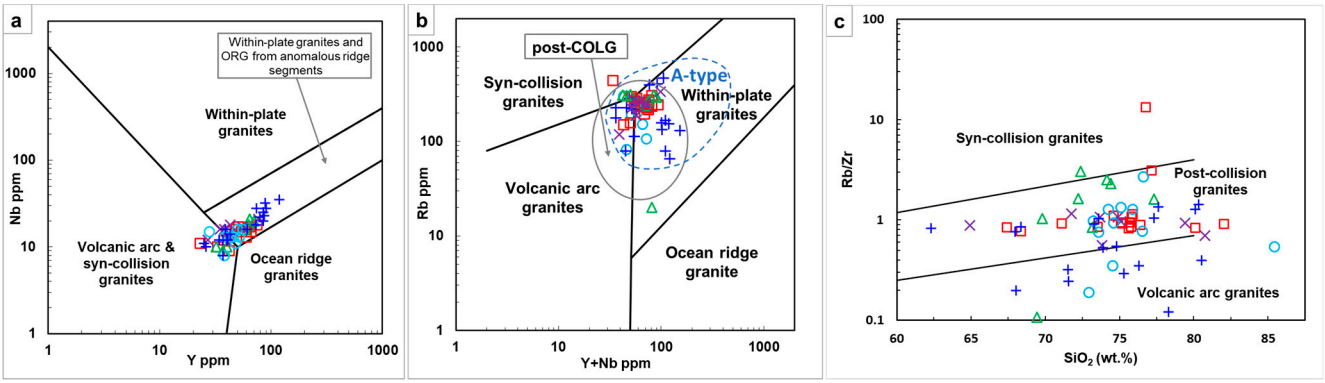

Figure 12. Tectonic discrimination diagrams for granites. (**a**) Y vs. Nb and (**b**) Nb + Y vs. Rb [112] with post-COLG (post-collision granites) field [113]. The A-type granites field in (**b**) is after [27]. (**c**) SiO_2 vs. Rb/Zr diagram [114]. Symbols are as in Figure 4.

Eby [29,101] divided A-type granitoids into two chemical groups or subtypes, A1 and A2, based on their tectonic setting. The A1-subtype represents granitoids formed in true anorogenic rifting (within-plate), while the A2-subtype corresponds to post-collisional granitoids. He considered the Y/Nb ratio as a key indicator for distinguishing between these groups. A1 granitoids have Y/Nb < 1.2 and are mantle-derived, whereas A2 granitoids exhibit Y/Nb > 1.2 and are crust-derived. All samples of the CRB silicic volcanic rocks have Y/Nb ratios exceeding 1.2 (1.87–4.75; average 3.36) (Table S1) and therefore plot well in the A2 group field (Figure 13) on the Nb–Y–Ce and Nb–Y–Zr/4 ternary diagrams and on the Y/Nb vs. Rb/Nb or Sc/Nb discrimination diagrams of Eby's [29], implying extrusion in a post-collisional environment and dominant crustal magma sources derivation, as discussed in the next subsection.

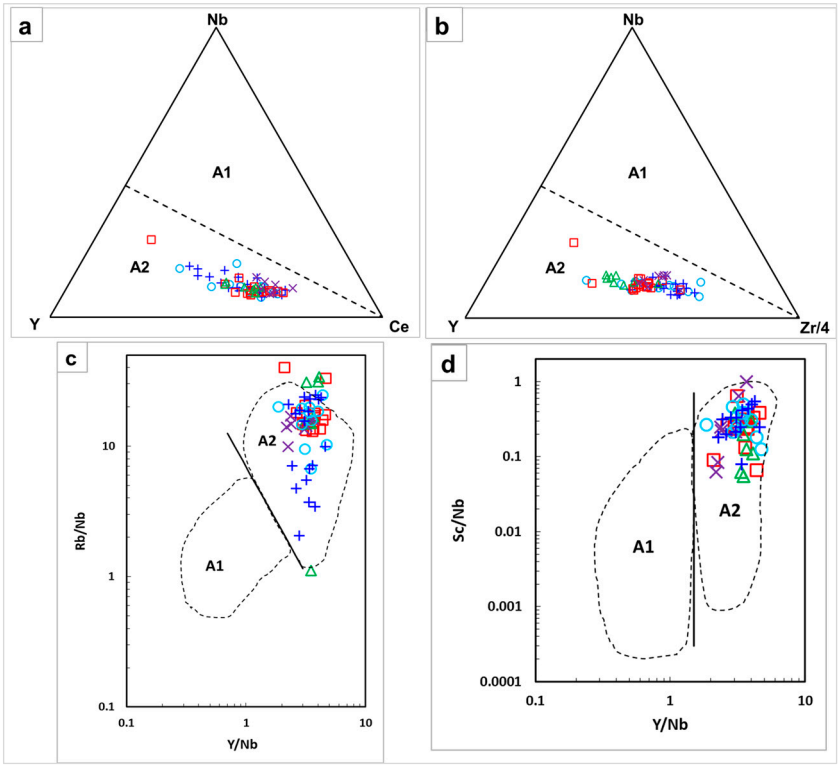

Figure 13. Plots of the CRB silicic volcanic rocks on (**a**) Nb–Y–Ce and (**b**) Nb–Y–Zr/4 ternary diagrams (the dashed line represents Y/Nb ratio = 1.2) as well as on (**c**) Y/Nb vs. Rb/Nb and (**d**) Y/Nb vs. Sc/Nb discrimination diagrams for the subdivision of the A-type granitoids into A1 (anorogenic within-plate) and A2 (post-collision) groups or subtypes [29]. Symbols are as in Figure 4.

6.3. Petrogenesis and Magma Sources

6.3.1. Source Material: Crustal Versus Mantle Contributions

Various petrogenetic models have been suggested to explain the origin of A-type granitic melts. A-type granitoids can be produced mainly from three fundamentally different petrogenetic schemes concerning different processes and various sources: (1) direct fractionation of mantle-derived alkaline or tholeiitic magmas (e.g., [29,30,99,101,115]); (2) partial melting of felsic crustal rocks (e.g., [27,29,97,101,104,116–120]); and (3) a combination of the previous two models in which mantle-derived mafic magma is mixed with crust-derived felsic magma and/or undergoes assimilation by crustal rocks (e.g., [27,29–31,97,104,116,117,121–125]). The challenge is to determine which of these pathways was followed.

The first model, which involves the direct extensive fractionation of mantle-derived alkaline or tholeiitic magma, is precluded due to the lack of field evidence for significant volumes of the associated Akritas–Metallikon basic rocks and the absence of a compositional continuum that this process would typically produce. However, an association with tholeiitic mafic rocks is a typical feature of A-type granites, and it is generally accepted that mantle-derived magmas act as the heat source for crustal partial melting, leading to the production of large volumes of silicic A-type magmas (e.g., [31,116,126–130]). This is discussed in more detail in Section 6.5.

In the following, an attempt is made to estimate the contribution of the crust versus the mantle in generating the A-type CRB silicic volcanic rocks using whole-rock geochemical data. Some diagnostic trace element ratios, such as Y/Nb, Ce/Nb, Th/Nb, La/Nb, Ce/Pb, Rb/Sr, and Rb/Nb, are considered as well.

The strong peraluminous nature (average A/CNK = 1.13) of the CRB silicic volcanic rocks, their enrichment in K, Rb, Th, and Pb, and their depletion in Ba, Sr, Nb, P, and

Ti (Figure 8) indicate that they are crust-derived rhyolites. The Y/Nb ratio in A-type granitoids, besides the tectonic discrimination, can be considered a diagnostic feature of magma sources. Eby [29,101] has inferred that the fractionation of A-type granitic magmas has little to no significant impact on the Y/Nb ratio, and mantle-derived granites (A1 group) exhibit low Y/Nb ratios (<1.2), whereas granites derived from crustal sources (A2 group) are characterized by higher Y/Nb ratios (>1.2). All samples from the CRB silicic volcanic rocks have Y/Nb ratios above 1.2 (Table S1, Figure 13) and belong to the A2 post-collisional group, as it has been previously demonstrated, implying dominant crustal sources. Additionally, the Ce/Nb vs. Y/Nb discrimination diagram is used to evaluate potential genetic relationships of A-type granitoids with crustal sources or mantle-derived magmas [29,101]. In this diagram (Figure 14), the CRB silicic volcanic rocks clearly do not plot in the OIB field (A1 group) but straddle a trend extending from bulk continental crust (black dot; [131]) to the IAB field, characteristic for the A2 group, suggesting not only their derivation through crustal anatexis but also the involvement of subduction- or continent–continent collision-related crustal components as magma sources [29,101].

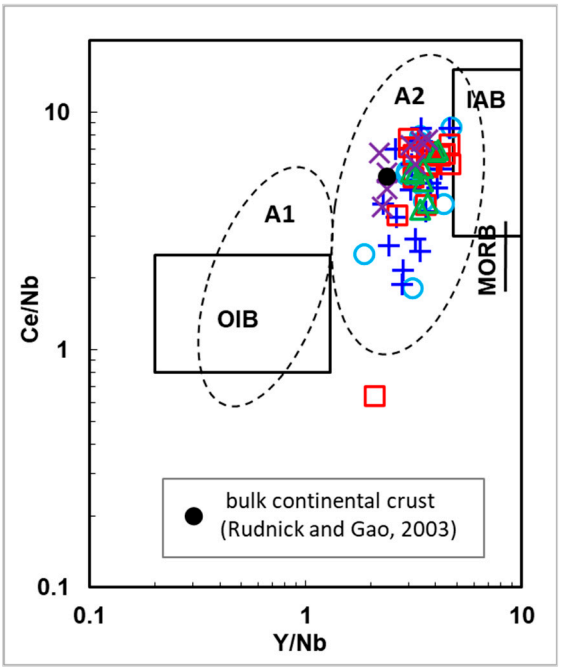

Figure 14. Ce/Nb vs. Y/Nb discrimination diagram to estimate possible genetic links of the CRB silicic volcanic rocks with crustal sources or mantle-derived magma. A1: mantle-derived granitoids and A2: crustal granitoids, IAB: Island-Arc Basalt, OIB: Ocean-Island Basalt, MORB: Mid-Ocean Ridge Basalt (the fields are from [29,101]), black dot: bulk continental crust [131]. Symbols are as in Figure 4.

The ratios Y/Nb, Th/Nb, La/Nb, and Ce/Pb, commonly used to characterize OIB and subduction-related magmatic suites, were applied to worldwide A-type granitoids by Moreno et al. [132,133] to investigate their magma sources and fractionation mechanisms. According to Moreno et al. [133], the relationships of the above-mentioned ratios in OIB and subduction-related magmatic suites suggest that A-type felsic rocks with normalized values of $(Th/Nb)_N < 1.3$, $(La/Nb)_N < 1.3$, and $(Ce/Pb)_N > 1$ are more likely to exhibit $(Y/Nb)_N < 0.18$, indicating A1-subtype affinity. In contrast, those with $(Th/Nb)_N > 2$, $(La/Nb)_N > 2$, and $(Ce/Pb)_N < 1$ generally show $(Y/Nb)_N > 0.18$, A2-subtype affinity and a significant additional contribution from crustal sources. On the $(Y/Nb)_N$ vs. $(Th/Nb)_N$ diagram of Moreno et al. [133], the rock samples plot within the A2-subtype continental crust field, which is distinct from the OIB field (Figure 15a). This is further supported by the

$(La/Nb)_N$ vs. $(Th/Nb)_N$, $(Ce/Pb)_N$ vs. $(Th/Nb)_N$, and $(La/Nb)_N$ vs. $(Ce/Pb)_N$ diagrams of Moreno et al. [133], where the compositional trends of the CRB silicic volcanic suite align with subduction-related magmatic suites, away from the OIB array (Figure 15b–d). This is explained by Eby's [29,101] crust-derived source model.

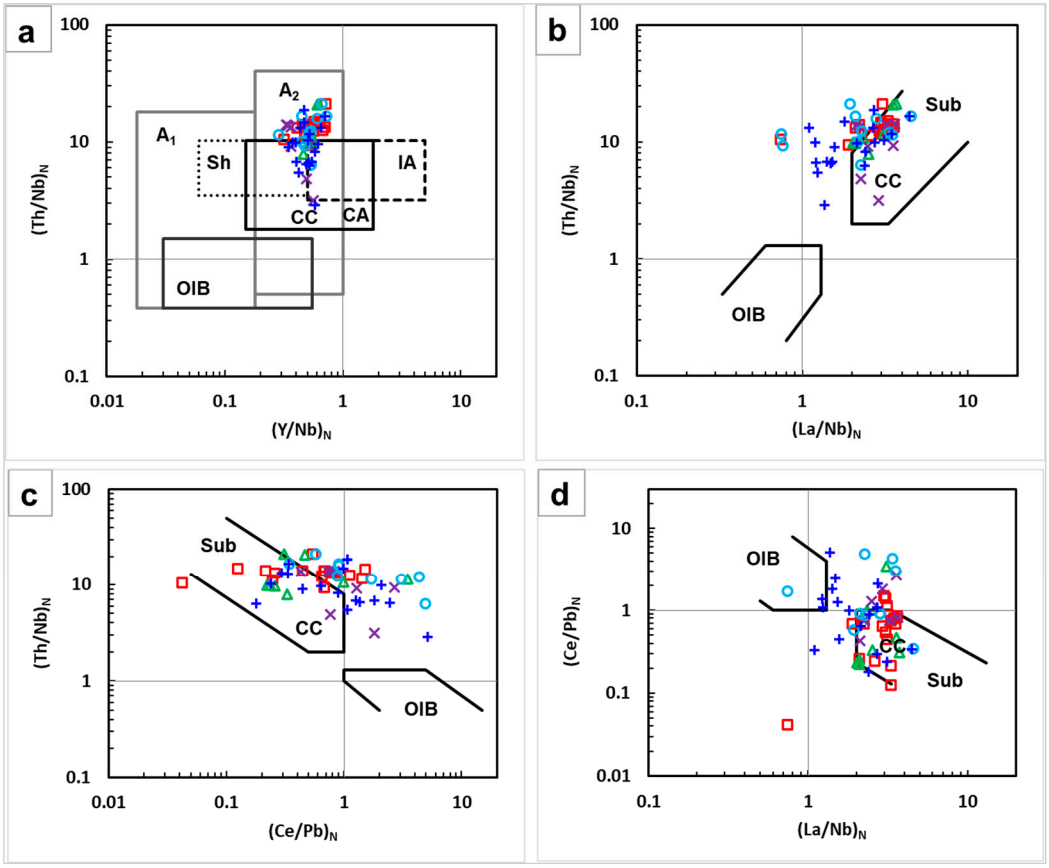

Figure 15. Compositional relationships between Y/Nb, Th/Nb, La/Nb, and Ce/Pb in the CRB silicic volcanic rocks. (**a**) $(Y/Nb)_N$ vs. $(Th/Nb)_N$, (**b**) $(La/Nb)_N$ vs. $(Th/Nb)_N$, (**c**) $(Ce/Pb)_N$ vs. $(Th/Nb)_N$, and (**d**) $(La/Nb)_N$ vs. $(Ce/Pb)_N$ discrimination diagrams with compositional fields after [133]. Values normalized to the silicate earth after [134]. A1: mantle-derived granitoids and A2: crustal granitoids, CC: continental crust, CA: continental arcs, OIB: ocean island basalt, IA: island arcs, Sh: shoshonites, Sub: subduction-related magmatic suites. Symbols are as in Figure 4.

Rb and Sr relative abundances provide insight into the place of magma generation. The CRB silicic volcanic rock samples exhibit a wide range of extremely high Rb/Sr ratios (3.45–39.14; average 15.8), which is attributed to their very low Sr concentrations (Table S1, Figure 9c). Considering the extremely low Rb/Sr ratio (0.01–0.1) typical of mantle materials [135], compared to the higher Rb/Sr ratios observed in the lower, middle, and upper continental crust (average 0.12, 0.22, and 0.32, respectively) [136,137], the very high Rb/Sr ratio of the CRB silicic volcanic rocks rules out a mantle contribution, indicating unequivocally crustal sources for their generation.

Additionally, crustal compositions and melts are characterized by a high Rb/Nb ratio (>2) [138], in contrast to upper mantle materials like N-MORB, which exhibit a low Rb/Nb ratio (<1). In a diagram using trace element ratios such as Nb/Y and Rb/Y [138], all the CRB silicic volcanic rock samples show a high Rb/Nb ratio (average = 16.2; Table S1) and plot near the upper and middle continental crustal values, except for some samples from the Akritas and Metallikon areas, which plot closer to the lower continental crustal values [131] (Figure 16).

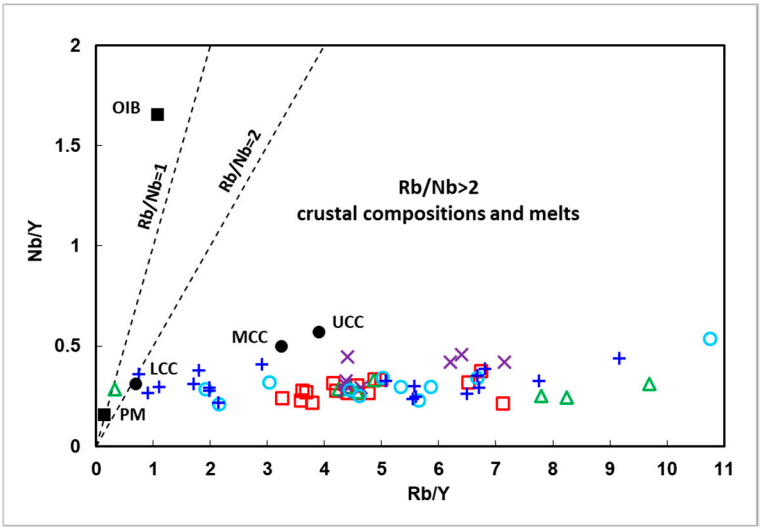

Figure 16. Nb/Y vs. Rb/Y diagram for the CRB silicic volcanic rocks (modified after [138]). The compositions of upper, middle, and lower continental crust (UCC, MCC, LCC) were taken from [131], and the compositions of primordial mantle (PM) and ocean island basalts (OIB) were taken from [98]. Symbols are as in Figure 4.

6.3.2. Crustal Protolith—Source Compositional Characteristics

Assuming a derivation of the peraluminous A-type CRB silicic volcanic rocks mainly from the partial melting of a crustal protolith, the source rock composition is further researched. Possible crustal source rocks feasible to produce peraluminous A-type granitoids include (1) anhydrous lower crustal granulites [27,104,116], (2) tonalitic–granodioritic gneisses [108,117,120,139,140] and (3) metasedimentary rocks (pelites and graywackes) [95,96,129,141–146], including also cases of basaltic magma admixture.

Experiments on melting have shown that the "residual" lower crustal sources cannot produce magmas with the geochemical features of A-type granites [117,118]. However, at high temperatures, A-type granites may be derived from the partial melting of granulitic metasedimentary rocks that remain in the lower crust following the extraction of an orogenic I-type granite [27,104,116,147]. This "residual-source model" is not appropriate for the generation of the A2-subtype CRB silicic volcanic rocks, as there is no evidence of existing I-type granite in the Vertiskos Unit basement (namely, the existing granites are S-type syn-collisional: the Polydendri meta-granite [77] and the Theodorio meta-granite [78]). In addition, the high Rb/Sr ratio (3.45–39.14; average 15.8) characterizing the CRB silicic volcanic rocks cannot be explained by partial melting of the typical granulite crustal rocks (average granulite Rb/Sr ratio: 0.023 [135]). Therefore, anhydrous lower crustal granulites are precluded as magma sources, and the partial melting of tonalitic–granodioritic gneisses or metasedimentary rocks (pelites and graywackes) is further investigated as a possible process for magma derivation.

Granitoid melts generated experimentally from different crustal source rocks by dehydration partial melting show distinct chemical characteristics, allowing the identification of compositionally diverse protoliths [140,148–151]. Thus, to constrain the possible source rocks of the CRB silicic volcanic rocks, appropriate major and trace element plots (e.g., [95,141,152]) are used.

The molar $Al_2O_3/(MgO + FeO_t)$ vs. molar $CaO/(MgO + FeO_t)$ diagram [152] distinguishes among partial melts derived from crustal sources such as metapelites, metagraywackes, and metatonalites. Based on this diagram, the A2-subtype CRB silicic volcanic suite appears to have originated from the partial melting of metapelitic source rocks (Figure 17a).

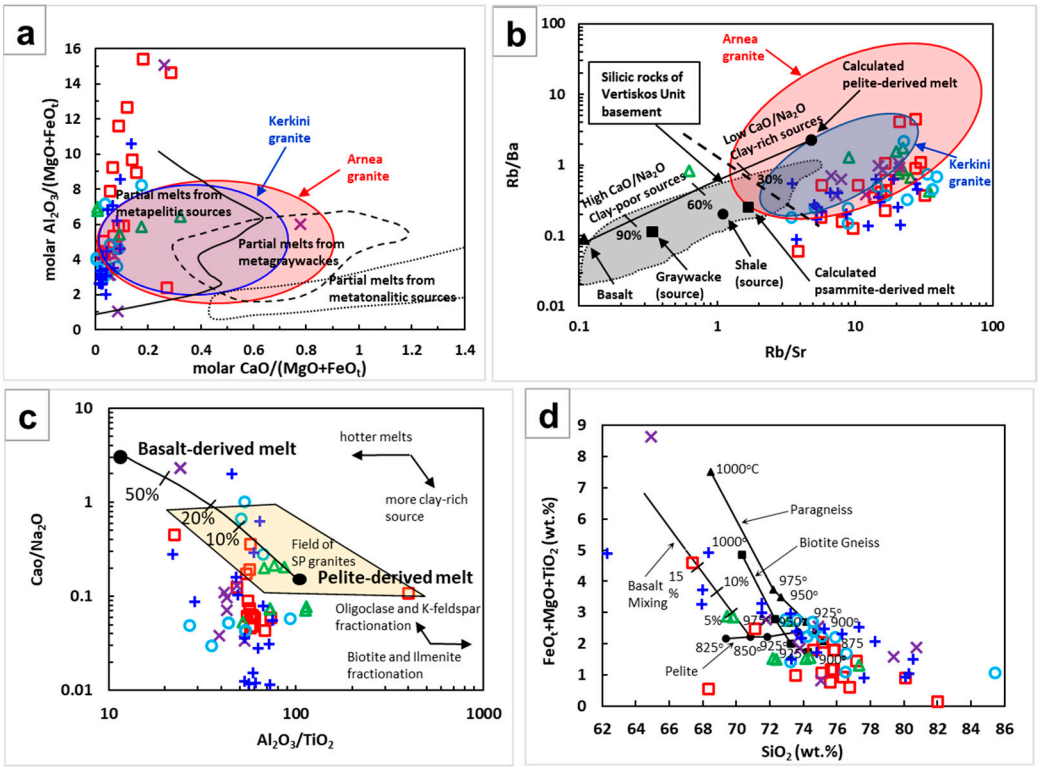

Figure 17. Source region discrimination diagrams for the post-collisional CRB silicic volcanic rocks: (**a**) molar $Al_2O_3/(MgO + FeO_t)$ vs. molar $CaO/(MgO + FeO_t)$ diagram [152], (**b**) Rb/Ba vs. Rb/Sr diagram [95]; the psammite- and pelite-derived melt compositions are produced from the calculation of [153] and the average composition of basalt, graywacke, and shale are of [154]. The gray field represents the felsic rocks (metapelites) from the Vertiskos Unit basement (the data are from [75,77,78]). The geochemical data for the Arnea and Kerkini granites are from [18,37,40]. (**c**) CaO/Na_2O vs. Al_2O_3/TiO_2 diagram (after [95]); the mixing curve between the average Phanerozoic basalt of [154] and the 850 °C, 10 kbar pelite-derived melt of [149] is also shown where percentages of basalt mixing are indicated. (**d**) (FeO_t + MgO + TiO_2) vs. SiO_2 diagram (after [95]). Temperatures of the experimental vapor-absent 10 kbar melts of natural pelite are after [149], of synthetic biotite gneiss are after [118], and of natural volcanoclastic paragneiss are after [155]. Symbols are as in Figure 4.

Rb–Sr–Ba variations in post-collisional strongly peraluminous (SP) granites suggest that both pelitic and psammitic sources significantly contributed to their genesis [95]. On the Rb/Sr vs. Rb/Ba diagram [95], which provides additional constraints on the magmatic source, the CRB silicic volcanic rocks exhibit a high Rb/Sr ratio and plot in the low CaO/Na_2O clay-rich source region (Figure 17b), revealing again a pelitic parentage.

Moreover, the CaO/Na_2O and Al_2O_3/TiO_2 ratios can be used to infer the source rock characteristics and partial melting temperatures of granitic magmas, respectively [95,156]. According to Sylvester [95], strongly peraluminous (SP) granitic melts originating from plagioclase-poor and clay-rich sources (i.e., pelites) tend to have lower CaO/Na_2O ratios (<0.3) than melts derived from plagioclase-rich and clay-poor ones (i.e., psammites). Furthermore, Jung and Pfander [156] found that CaO/Na_2O ratios can differentiate between granitic melts derived from pelites (CaO/Na_2O < 0.5) and those originating from graywackes or igneous sources (CaO/Na_2O ranging from 0.3 to 1.5). Under high-temperature conditions in the source region, biotite and ilmenite become unstable, leading to an increase in Ti content in the resulting melts [157]. Hence, the Al_2O_3/TiO_2 ratio reflects the melting temperature and is used as a geothermometer for given source compositions. Peraluminous granitic melts with low Al_2O_3/TiO_2 ratios will have been derived at higher temperatures than those with high Al_2O_3/TiO_2 ratios regardless of the source composi-

tion [95,156]. Therefore, using the discrimination diagram CaO/Na_2O vs. Al_2O_3/TiO_2 [95], magma sources can be further distinguished. Almost all the CRB silicic volcanic rock samples have a low CaO/Na_2O ratio (<0.5), with an average value of 0.21 (Table S1), which aligns with their origin from pelitic metasediments rather than metagraywackes (Figure 17c). Furthermore, all the CRB silicic volcanic samples are characterized by low Al_2O_3/TiO_2 ratios ranging from 16 to 113 (except sample KOL2) with an average value of 61 (Table S1, Figure 17c), indicating that the source underwent partial melting under high-temperature conditions.

The inverse correlation between SiO_2 and $FeO_t + MgO + TiO_2$ that the SP granites exhibit, according to Sylvester [95], is also obvious for the A2-subtype CRB silicic volcanic rocks (Figure 17d). Furthermore, the CRB silicic volcanic rock samples mostly plot in the clay rocks region (pelite), indicating mainly crustal pelitic components as the source rocks and 850–950 °C melting temperatures.

6.3.3. Magma Temperatures: Zircon Saturation Thermometry

The temperature of the felsic magma can be calculated from bulk rock compositions using the zircon saturation thermometry (T_{Zr}) developed by Watson and Harrison [158].

$$T_{Zr} = 12{,}900/[2.95 + 0.85M + \ln(496{,}000/Zr_{melt})]$$

where M is the molar cation ratio $[(Na + K + 2 \times Ca)/(Al \times Si)]$ of the whole-rock concentration of Na_2O, K_2O, CaO, Al_2O_3, and SiO_2.

According to Miller et al. [159], zircon saturation thermometry provides a reliable estimate of magma temperature during zircon crystallization. The uncertainty for the thermometer is ±24 °C.

The zircon saturation temperatures (T_{Zr}) obtained for the CRB silicic volcanic rocks from the five outcropping areas range almost between 800 and 1000 °C, yielding an average temperature of 886 °C, over a range of SiO_2 from 62.30 to 85.42 wt.%. The Akritas (T_{Zr} = 802–971 °C, average 884 °C) and Metallikon (T_{Zr} = 822–1007 °C, average 924 °C) rock samples have yielded a wider range of temperatures and higher averages compared to those of the Kolchida (T_{Zr} = 791–904 °C, average 875 °C; sample KOL2 has a value of 705 °C and is excluded as problematic), Nea Santa (T_{Zr} = 792–922 °C, average 846 °C), and Sana (T_{Zr} = 858–922 °C, average 884 °C) areas (Figure 18a,b, Table S1).

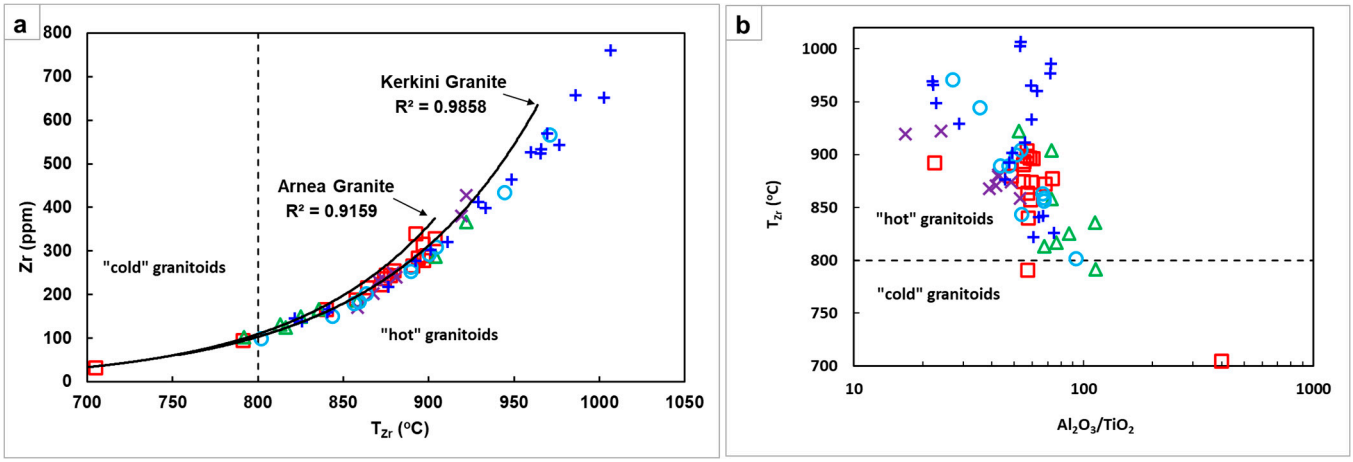

Figure 18. (**a**) T_{Zr} vs. Zr diagram for the CRB silicic volcanic rocks and comparison with the calculated T_{Zr} for the Arnea and Kerkini granite suites (after [159]). Estimated whole-rock zircon saturation temperatures (T_{Zr}) were calculated using the equation introduced by [158]. (**b**) Al_2O_3/TiO_2 vs. T_{Zr} diagram for the CRB silicic volcanic rocks (after [160]). Symbols are as in Figure 4.

There are two distinct groups of granitoids generated at different temperatures: (1) the "hot" (T_{Zr} > 800 °C) inheritance-poor and (2) the "cold" (T_{Zr} < 800 °C) inheritance-rich granitoids [159]. The investigated CRB silicic volcanic rocks are inferred to be equivalents of "hot" zircon inheritance-poor granitoids (T_{Zr} between 800 and 1000 °C; Figure 18a,b), suggesting that their initial magmas were undersaturated in zircon at the source. Therefore, the calculated zircon saturation temperatures (T_{Zr}) provide a minimum magmatic temperature estimate at the source and are likely to be an underestimate of their initial temperature [159,161]. These high values of temperature are consistent with those of A-type granites [97,116,158,162], further suggesting that the CRB silicic volcanic rocks belong to A-type granitic magmas.

According to Bucholz and Spencer [160], SP granites with low Al_2O_3/TiO_2 ratios (<100) exhibit higher Zr contents (>100 ppm) and Zr saturation temperatures (average 807 °C), while those with high Al_2O_3/TiO_2 ratios (>100) display lower Zr contents (<100 ppm) and Zr saturation temperatures (688 °C). The relatively high Zr concentrations (>100 ppm) and consequently the estimated high zircon saturation temperatures (T_{Zr} > 800 °C, average 886 °C) of the CRB silicic volcanic rocks are consistent with their low Al_2O_3/TiO_2 ratio (<100), implying a significant degree of partial melting of their metasedimentary protolith (Figure 18b).

6.3.4. Comparison of the CRB Silicic Volcanic Rocks to the Related Arnea and Kerkini Granites

The Permo–Triassic A-type Arnea and Kerkini granites, which intruded into the Vertiskos Unit (Variscan basement), are considered the deep-level counterparts of the investigated CRB silicic volcanic rocks [18,19], as their similar age and geochemical characteristics suggest a genetic link between them (see also Figure 15 in [18]). Geochemical studies on the Arnea and Kerkini granites consider them as A2-subtype post-collisional granites [18,41]. This outcome is consistent with the results of this study for the CRB silicic volcanic rocks.

Poli et al. [18], based on the quite similar Rb, Ba, and Sr values of the A2-subtype Arnea and Kerkini granites, inferred that their magma was likely derived from the partial melting of the same source (continental crust). Excluding the metasedimentary source and based on the normative Q–An–Ab–Or plots and the molar $Al_2O_3/(Na_2O + K_2O + CaO)$–$K_2O/Na_2O$–$FeO/MgO$ ternary diagram, they conclude that the probable origin involves the partial melting of tonalitic sources. Nevertheless, on the molar $Al_2O_3/(MgO + FeO_t)$ vs. molar $CaO/(MgO + FeO_t)$ diagram [152], the Arnea and Kerkini granites (geochemical data from [18,37,40]) plot within the area of partial melts derived from crustal sources such as metapelites and metagraywackes rather than metatonalites (Figure 17a). Moreover, on the Rb/Sr vs. Rb/Ba diagram [95], they occupy an area close to pelite-derived melts rather than psammite-derived ones, indicating magma sources similar to those of the CRB silicic volcanic rocks (Figure 17b) and reinforcing the idea of their genetic relationship.

Regarding magma temperatures, the calculated T_{Zr} values (geochemical data from [18,37,40]) for the Arnea granite range from 714 to 904 °C, with an average of 802 °C, while those for the Kerkini granite range from 753 to 964 °C, with an average of 884 °C, classifying them as "hot" granites. Equivalents of the "hot" granites commonly erupt [159], and the high T_{Zr} values of the Arnea and Kerkini granites, combined with their A2-subtype characteristics [18,41], support the assumption that they represent the plutonic roots of the CRB silicic volcanic rocks. The solubility of zircon as a function of temperature [159] for the melt composition of the CRB silicic volcanic rocks is compared to that of the Arnea and Kerkini granite suites in the T_{Zr} vs. Zr diagram (Figure 18a). It is observed that the Akritas–Metallikon silicic volcanic rocks align more closely with the Kerkini granite,

while the Kolchida–Nea Santa–Sana silicic volcanic rocks correspond better with the Arnea granite, which is an observation consistent with their spatial distribution (Figure 1).

6.3.5. Melting of the Palaeozoic Variscan Crust Basement (Vertiskos Unit) as Protolith

All of the above observations are consistent with the derivation of the Permo–Triassic peraluminous rhyolites of the CRB, along with the spatially and temporally associated Arnea and Kerkini granites, primarily from clay-rich and plagioclase-poor magma sources such as pelites. Potential parent pre-Triassic Variscan basement rocks are present in the area. The abundance of gneisses (metapelites) containing muscovite, biotite, garnet, and other aluminosilicate minerals in the nearby Variscan Vertiskos Unit basement [75,77,78], intruded by the Arnea and Kerkini granites, supports this assumption. Hence, the metapelites from the Palaeozoic Vertiskos Unit are likely sources for the generation of the CRB rhyolitic magma. A geochemical correlation between the Vertiskos metapelites and the studied CRB silicic volcanic rocks, as well as the Arnea and Kerkini granite intrusions, is attempted to establish them as feasible protoliths for partial melting.

In the Rb/Sr vs. Rb/Ba diagram (Figure 17b), the melting relationships between calculated melts and protoliths (average compositions) are illustrated [95]. Quartz, sillimanite, and garnet do not significantly incorporate Rb, Sr, and Ba [153]. Therefore, the increase in Rb/Sr and Rb/Ba ratios in the calculated pelite-derived melt, compared to the shale parent, is primarily determined by the amount of residual plagioclase and K-feldspar [95]. Thus, the observed increase in the Rb/Sr and Rb/Ba ratios in the studied CRB rhyolites, as well as in the Arnea and Kerkini granites (data from [18,37,40]), relative to that in the Vertiskos metapelites (data from [75,77,78]), enhances the idea that they are the protoliths of the A2-subtype silicic magma.

Some studies have shown that granitic melts formed by the partial melting of crustal rocks preserve or increase LILEs/HFSEs ratios during crustal anatexis, as LILEs (e.g., Rb) are more incompatible than HFSEs (e.g., Nb, Zr) [163–166]. The incompatible trace element ratios in the CRB silicic volcanic rocks, particularly LILEs/HFSEs (e.g., Rb/Nb: range 1.11–40, average 16.21; Rb/Zr: range 0.09–13.33, average 1.18; Th/Nb: range 0.38–2.56, average 1.42), are almost the same as those in the silicic Palaeozoic Variscan basement rocks of the Vertiskos Unit (gneisses data are from [75,77,78]), as is shown selectively in the Rb/Nb vs. Rb diagram (Figure 19a). Therefore, these distinct trace element ratios confirm the possibility that the melting occurred at a crustal level and provide additional evidence that the studied A2-subtype silicic magmatism was derived by the partial melting of the Palaeozoic Variscan Vertiskos Unit basement. This petrogenetic model is further supported by a plot of Nb/Y vs. Th/Y [127], in which the CRB rhyolite samples are positioned near the Th/Nb = 1 trend (Figure 19b), close to the average composition of the middle and upper continental crust [131], and plot within the field of the Vertiskos Unit (data are from [75,77,78]).

In conclusion, all these distinct trace element ratios confirm the possibility that the gneisses (metapelites) of the Palaeozoic Variscan Vertiskos Unit basement could be ideal magma sources for the A2-subtype CRB silicic volcanic rocks and their Arnea and Kerkini granitic suite counterparts.

To determine the depth of magma generation, the average Nb/Y, Rb/Y, Rb/Nb, Th/Y, and Th/Nb ratios of upper, middle, and lower continental crust (UCC, MCC, LCC) [131] are compared with the CRB silicic volcanic rocks data (Figures 16 and 19). Almost all the samples have values greater than that of the middle and upper crust, revealing shallow depths of magma generation. Furthermore, considering that the average Rb/Sr ratios of the upper, middle and lower continental crust are 0.26, 0.23, and 0.03, respectively [131], the high Rb/Sr ratio values (3.45–39.14; average 15.8) of the studied CRB silicic volcanic

rocks (Table S1, Figure 9c) imply a shallow depth of magma generation within the continental crust. Condie [167] used the relationship between Rb and Sr to determine crustal thickness, which increases with rising Rb and Sr contents. He also constructed a diagram to estimate the crustal depth at which the granitic magma was generated. Using this diagram (Figure 20), the data points of the CRB silicic volcanic rocks, as well as those of the Arnea and Kerkini granites (geochemical data from [18,37,40]), fall into the 20–30 km crustal thickness category, indicating relatively shallow to moderate depths of generation for this A2-subtype magma and granite emplacement. These depths correspond to pressures between 0.5 and 0.8 GPa.

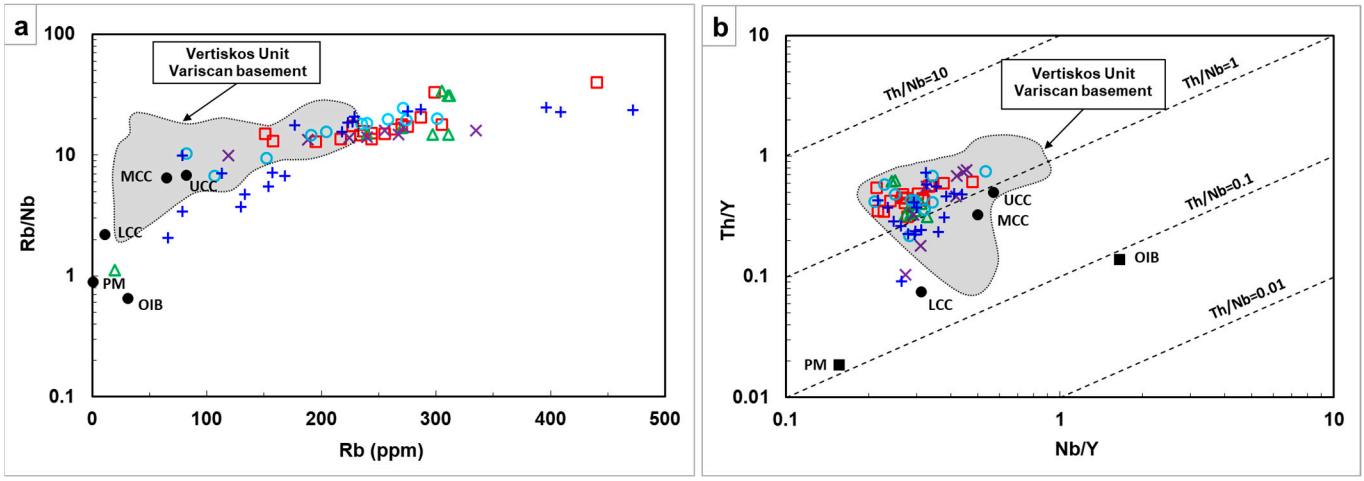

Figure 19. Variation diagrams for incompatible element ratios: (**a**) Rb/Nb vs. Rb and (**b**) Nb/Y vs. Th/Y. Data for the Palaeozoic Variscan basement (Vertiskos Unit gneisses) are from [75,77,78]. The compositions of upper, middle, and lower continental crust (UCC, MCC, LCC) were taken from [131]. The compositions of primitive mantle (PM) and ocean island basalt (OIB) were taken from [98]. Symbols are as in Figure 4.

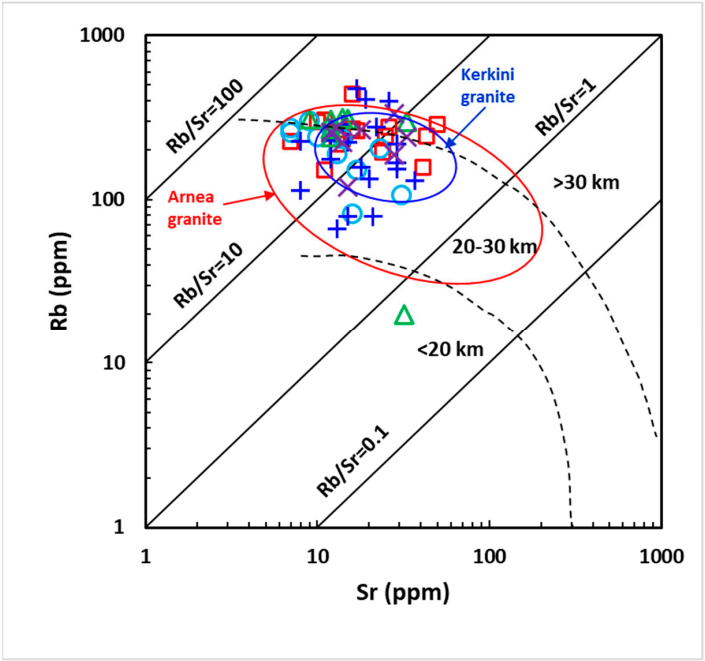

Figure 20. Rb–Sr binary diagram showing the distribution of the CRB silicic volcanic rocks along with the fields for the Arnea and Kerkini granites (geochemical data from [18,37,40]). The dashed lines represent crustal thickness separation areas (in kilometers), as inferred from the Rb–Sr crustal thickness index (after [167]). Symbols are as in Figure 4.

6.4. Mechanism of Crustal Anatexis and T-P Melting Conditions

6.4.1. Dehydration Melting

Peraluminous granites can be derived by the partial melting of crustal rocks under either fluid-absent or water-present conditions [150,168–171]. Melts produced in water-present conditions generally exhibit higher CaO and Na_2O and lower K_2O content, leading to higher normative anorthite (An) and albite (Ab) and lower orthoclase (Or) content. This results in melts with more tonalitic to trondhjemitic composition compared to the granitic melts produced under fluid-absent conditions [172,173]. The peraluminous CRB silicic volcanic rocks are characterized by high K_2O content and a K_2O/Na_2O ratio greater than 1.0 (Table S1). Their composition is predominantly granitic rather than tonalitic or trondhjemitic, as they have higher normative Or relative to An and Ab content (Table S1), which is inconsistent with melting under water-present conditions. In addition, the high zircon saturation temperatures (T_{Zr}) [158] of the CRB peraluminous rhyolites (Table S1, Figure 18) suggest that added water is not required for their production by the partial melting of pelitic metasediments, thus indicating that magma was generated under fluid-absent conditions.

This inference is further supported by the high values of Rb/Sr ratio (ranging between 3.45 and 39.14) of the CRB silicic volcanic rocks (Table S1, Figure 9c). In primary melts, the Rb/Sr ratio can be linked to the availability of fluids during the process of partial melting. Harris et al. [174] found that Rb/Sr ratios from 4 to 10 suggest magma formation under fluid-absent conditions (dehydration melting), while Rb/Sr ratios below 3.5 are indicative of magma genesis at water-present conditions. Consequently, the primary melts of the CRB silicic volcanic rocks were derived by fluid-absent melting conditions, since most of the samples have Rb/Sr ratios > 3.5. The negative Eu anomaly of their plutonic counterparts, i.e., the Arnea and Kerkini granitic suites [18,37], enhances the aspect for fluid-absent melting of the Variscan Palaeozoic Vertiskos crust.

6.4.2. Biotite or Muscovite Breakdown?

The dehydration melting of hydrous minerals in pelitic and felsic metamorphic rocks primarily depends on the muscovite and biotite, which supply all the water to the reaction systems. Experiments show that the fluid-absent melting of two-mica pelites during prograde metamorphism begins with the breakdown of muscovite and continues with the progressive breakdown of biotite [151,175,176]. At pressures of 0.5–1.0 GPa, muscovite breakdown begins at temperatures of 720–770 °C [175], while biotite breakdown occurs at 760–830 °C [142,177]. The high Zr concentrations (>100 ppm) and the high zircon saturation temperatures (average T_{Zr} = 886 °C) of the CRB silicic volcanic rocks, coupled with their low Al_2O_3/TiO_2 ratio (<100), were most probably obtained through relatively high-temperature dehydration melting above the biotite-breakdown curve (>800 °C).

Furthermore, during muscovite-dehydration melting, significant amounts of Pb are incorporated into the melt phase, while much of the Ba remains in the restite assemblage, which contains biotite and K-feldspar [178]. Therefore, the melts produced at low temperatures by the dehydration melting of muscovite are typically enriched in Pb relative to Ba. The logarithmic Pb vs. Ba diagram is useful for distinguishing primary low-temperature (<800 °C) S-type granites, formed by low-degree source melting (primarily muscovite melting), from high-temperature (>800 °C) S-type granites and secondary low-temperature S-type granites formed through fractionation [178]. In the Pb vs. Ba plot (Figure 21a), it is showed that the peraluminous CRB silicic volcanic rocks have relatively low Pb (0–69 ppm; average value 14 ppm) and high Ba (24–2929 ppm; average value 635 ppm) contents (low Pb/Ba ratio 0.00–0.27; average value 0.06), which resemble the high-temperature S-type granites generated by the dehydration melting of crustal rocks involving biotite breakdown.

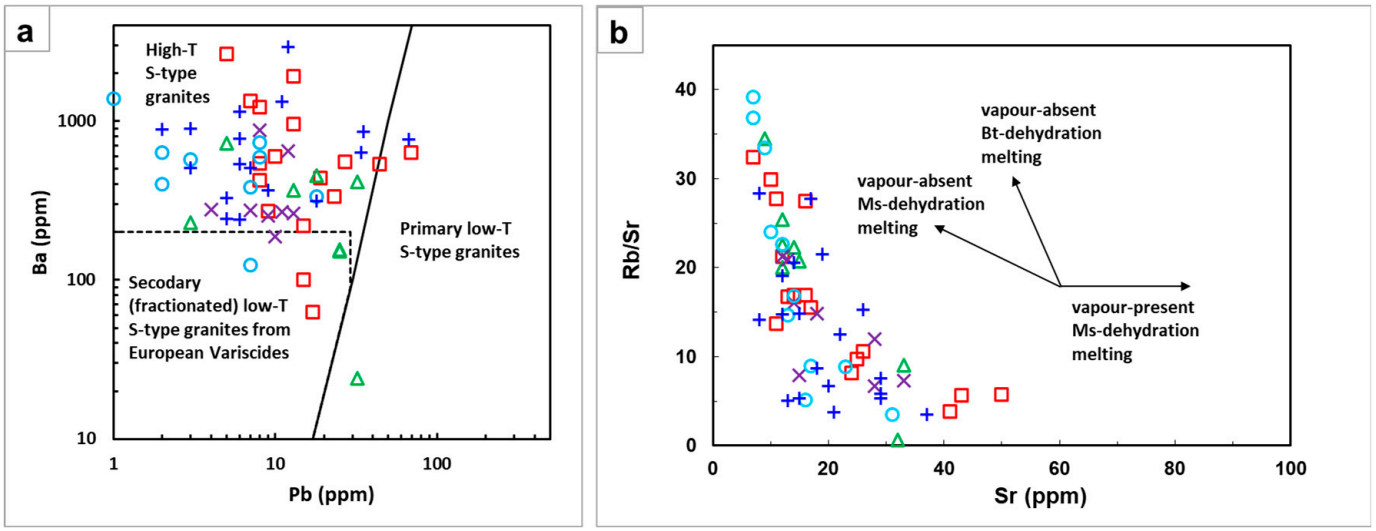

Figure 21. (**a**) Log–log plot of Pb vs. Ba displaying data for the CRB silicic volcanic rocks. The solid line empirically delineates the field occupied by the high-T (>800 °C) S-type granites from the European Variscides and the Lachlan Fold Belt from the primary low-T (<800 °C) S-type granitic magmas such as the Himalayan granites [178]. (**b**) Rb/Sr vs. Sr diagram [172]. Symbols are as in Figure 4.

Moreover, the dehydration melting of biotite significantly increases the Rb/Sr ratio in the melt while having minimal impact on Ba or Sr, as these elements are primarily contained in plagioclase [172]. The elevated Rb/Sr ratio in the CRB silicic volcanic rocks, evident in the Rb/Sr versus Sr diagram (Figure 21b), indicates that the rocks were predominantly generated by biotite melting under fluid-absent conditions.

6.4.3. Mineral Constituents in the Source Residue

The dehydration melting of biotite in metasedimentary rocks leads to the production of S-type granitic melts and the formation of residual granulite facies rocks (e.g., [148,179,180]). The pelite-derived melt under fluid-absent conditions is produced through the incongruent melting of all biotite and the majority of plagioclase via the following reaction:

Bt + Pl + Als + Qtz = Kfs ± Grt + melt [95,148,153,177,181] (Figure 22).

Residual orthopyroxene is also produced from graywacke partial melting [182,183]. The melting pressure determines the presence of plagioclase and garnet as common residual mineral phases. At relatively low pressure, plagioclase remains in the residual phase, whereas at higher pressure, garnet is retained in the residual phase (e.g., [184,185] and references therein). Moreover, at low pressures (below about 4 kbar), cordierite may replace garnet as a restite phase.

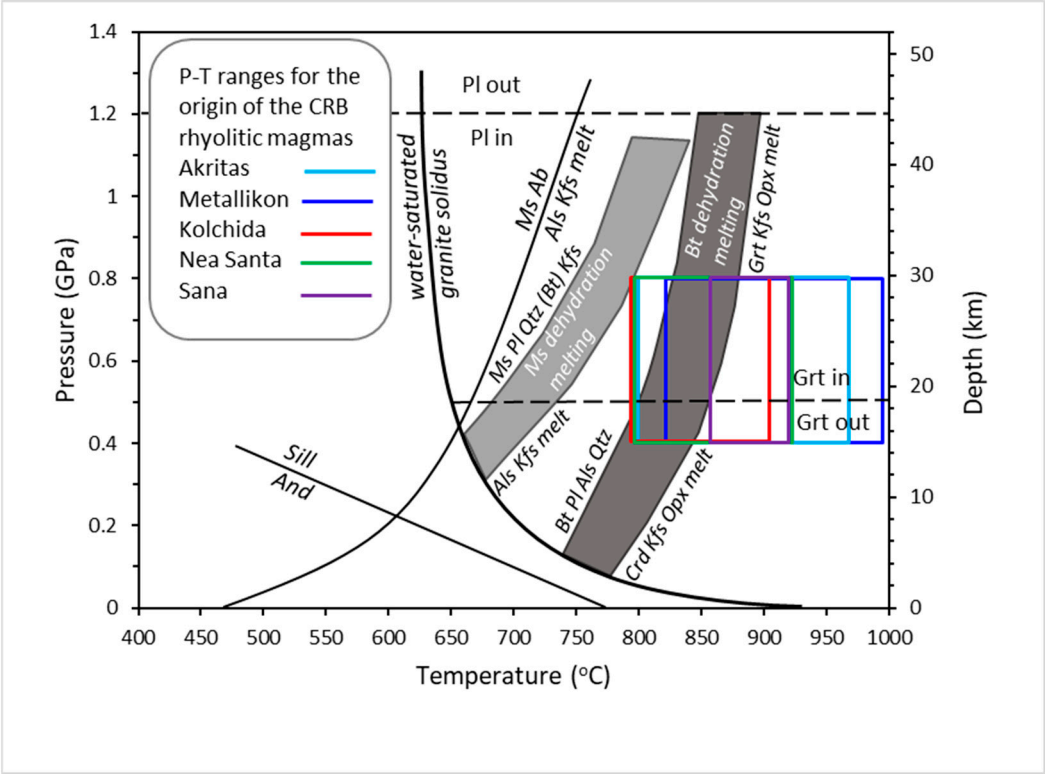

Figure 22. Pressure (P)–temperature (T) phase diagram (after [186]) showing probable conditions for the generation of the CRB rhyolitic magmas. Water-saturated granite solidus is from [187]. The light and dark gray fields represent the range of experimentally determined dehydration melting reactions for muscovite and biotite, respectively (after [175,182,188] and references therein). The lower pressure limit for garnet stability is after [175,188–190]. The upper pressure limit for plagioclase stability is after [191–193] (Ms: muscovite, Bt: biotite, Qtz: quartz, Pl: plagioclase, Ab: albite, Kfs: K-feldspar, Als: aluminosilicate, Grt: garnet, Crd: cordierite, Opx: orthopyroxene, Sill: sillimanite, And: andalusite).

The Rb/Sr ratio in the melt is greatly affected by the mineralogical composition of the residue after partial melting. Specifically, as Rb is retained by biotite and Sr is retained by the feldspars, the Rb/Sr ratio is increased in the melt by the presence of plagioclase and decreased by the presence of biotite in the residue [194]. The increase in Rb/Sr and Rb/Ba ratios in the CRB silicic volcanic rocks, as well as in the Arnea and Kerkini granitic suites, relative to the parental Vertiskos metapelites, indicates that plagioclase is retained in the source residue (Figure 17b). Plagioclase is enriched in Sr and Eu, whereas garnet is enriched in Y and HREEs (e.g., Yb) and depleted in LREEs (e.g., La). Therefore, the Sr and Eu anomalies, as well as the Sr/Y and La/Yb values, are often used to estimate the presence of these residual phase minerals in the source and consequently the melting pressure (e.g., [184]). The pronounced negative Sr anomalies in the primitive mantle-normalized trace element patterns (Figure 8), along with the very low Sr/Y ratios (0.12–1.08; average 0.37) in the CRB silicic volcanic rocks (Table S1), suggest that the magma source residue was dominated by plagioclase with little or no garnet. This indicates relatively low pressures (<7 kbar [150]) and a shallow magma origin.

The geochemically similar Permo–Triassic counterparts, the Arnea and Kerkini granites [18], which intruded the Vertiskos Variscan Unit basement, exhibit strongly negative Eu and Sr anomalies [18,37]. According to Poli et al. [18], the low Sr content and unfractionated HREEs (flat pattern) suggest their generation from sources containing residual feldspars but lacking garnet, indicating lower pressures and depths of less than 50 km for magma generation. Moreover, the low Sr/Y (0–4) and La/Yb (2.5–10) ratio values in the Arnea

and Kerkini granites (geochemical data from [18,37,40]) are consistent with crustal melts formed within the stability field of residual plagioclase with little or no residual garnet (the F3 field in the Sr/Y vs. La/Yb diagram of [185]). This result supports the idea of a shared magma source at relatively low pressure and shallow depth for the CRB silicic volcanic rocks and the spatially and temporally associated Arnea and Kerkini granites.

6.4.4. Pressure–Temperature Melting Conditions and Melt Proportions

The pressure (P)–temperature (T) conditions for the partial melting of crustal rocks are outlined in Figure 22, based on experimental data (after [186]). It is indicated that at pressures of 0.5–1.0 GPa, muscovite begins to break down at temperatures of 720–770 °C [175] and biotite breakdown occurs at 760–830 °C [142,177]. Furthermore, experimental data suggest that garnet is formed at pressures between 0.4 and 0.6 GPa and temperatures ranging from 750 to 900 °C during the fluid-absent partial melting of metasedimentary rocks [157,175,184,189]. This suggests that the lower pressure limit for garnet stability is around 0.5 GPa. Plagioclase is a typical residual mineral during the partial melting of various crustal rocks—including metasedimentary rocks, tonalites, and basalts—but it disappears at pressures exceeding 1.2 to 1.5 GPa (e.g., [191–193]).

Considering the evidence of residual plagioclase with little or no residual garnet in the source, it is concluded that the CRB rhyolitic, as well as the Arnea and Kerkini granitic magmas, were produced by the biotite dehydration melting of metapelites over a range of pressures from 0.4 to 0.8 GPa. These pressures correspond to depths of ~15–30 km, which is consistent with the depth level inferred from the Rb–Sr crustal thickness index [167] and furthermore suggesting crustal thinning of the Vertiskos Unit basement during the Permo–Triassic. Moreover, taking into account that the zircon saturation temperature (T_{zr}) values for the CRB silicic volcanic rocks are in the range of 800 to 1000 °C, it is inferred that the rocks formed at high temperatures within this range. However, the maximum melting temperature may have been lower than 1000 °C, as some samples with high Zr content from the Metallikon area may have been derived from magma mixing (work in progress). The pressure (depth)–temperature range field for the CRB silicic volcanic rocks is drawn on the P–T diagram (Figure 22).

Melt proportions produced by crustal partial melting primarily depend on the type of source rock, the pressure, the temperature, and the source's hydrous mineral (H_2O) content. Clemens and Vielzeuf [181] developed models linking the maximum melt production from pelites and quartzofeldspathic rocks to the water content in hydrous minerals. Pelites and felsic rocks containing approximately 1 wt.% total water at 0.5 GPa can generate about 30 vol.% melt at 800 °C and 60 vol.% melt at 900 °C (see Figure 4 in [181]), whereas at 1 GPa, they can form about 18 vol.% and 35 vol.% melt at 800 °C and 900 °C, respectively. According to the Clemens and Vielzeuf model for the partial melting of pelites [181], the melt fraction produced from the partial melting of the Vertiskos Unit basement at temperatures of 800–1000 °C and pressures of 0.4–0.8 GPa (approximately 15–30 km depth) is estimated to range from 35 to 60 vol.%.

6.5. Heat Source for Crustal Melting and Petrogenetic Model

The magma of the CRB silicic volcanic rocks was essentially produced by crustal melting inside the Palaeozoic Vertiskos Unit basement at a relatively shallow depth between the mantle roof (~30 km, 0.8 GPa) and just below the lower limit of garnet stability (~15 km, 0.4 GPa) at temperatures up to 1000 °C. Such high temperatures are uncommon in the crust, indicating the need for an additional heat source. This suggests the involvement of mantle-derived magmas at the base or into the lower part of the crust [29,95,159]. Supporting evidence for basaltic underplating magmatism is provided by the nearby

minor outcrops of the Triassic Akritas–Metallikon tholeiitic basalt and dolerite displaying transitional MORB to WPB characteristics (the Triassic Rift Basic Volcanics [16,43,44,46]). Additionally, the presence of limited magma mixing microtextures in dacites and mafic microgranular enclaves in rhyolites from the Metallikon area provides further evidence of coexisting mafic and felsic volcanism [45]. The calculated P–T conditions for the basic tholeiitic magma generation (1219–1342 °C, 1.01–1.61 GPa) imply a depth lower than 50 km corresponding to a spinel-peridotite source [46]. The tholeiitic magma may have formed through adiabatic decompression and melting of an upwelling asthenosphere. Such upwelling can be triggered by various tectonic processes, including convective thinning of the lithospheric mantle, lithosphere delamination, or slab break-off ([129,195] and references therein). Therefore, it is concluded that the Triassic volcanism in the CRB was in fact bimodal (A2-subtype rhyolites to rhyodacites and minor tholeiitic basalts) and formed in a post-collision extensional tectonic setting (e.g., [130,195–200]).

In Figure 23, the diagram illustrates the petrogenetic model for the Permo–Triassic CRB silicic volcanic rocks and the Akritas–Metallikon tholeiitic basalts that were generated in a post-collision extensional stage of the Variscan continental crust. Plutonic equivalents of similar age and geochemistry that have been intruded into the crystalline basement of the Vertiskos Unit are the A-type Arnea and Kerkini meta-granites (254–244 Ma and 247 Ma, respectively [17,18,39]) and the MORB Volvi meta-mafic body (240 Ma [20,201]).

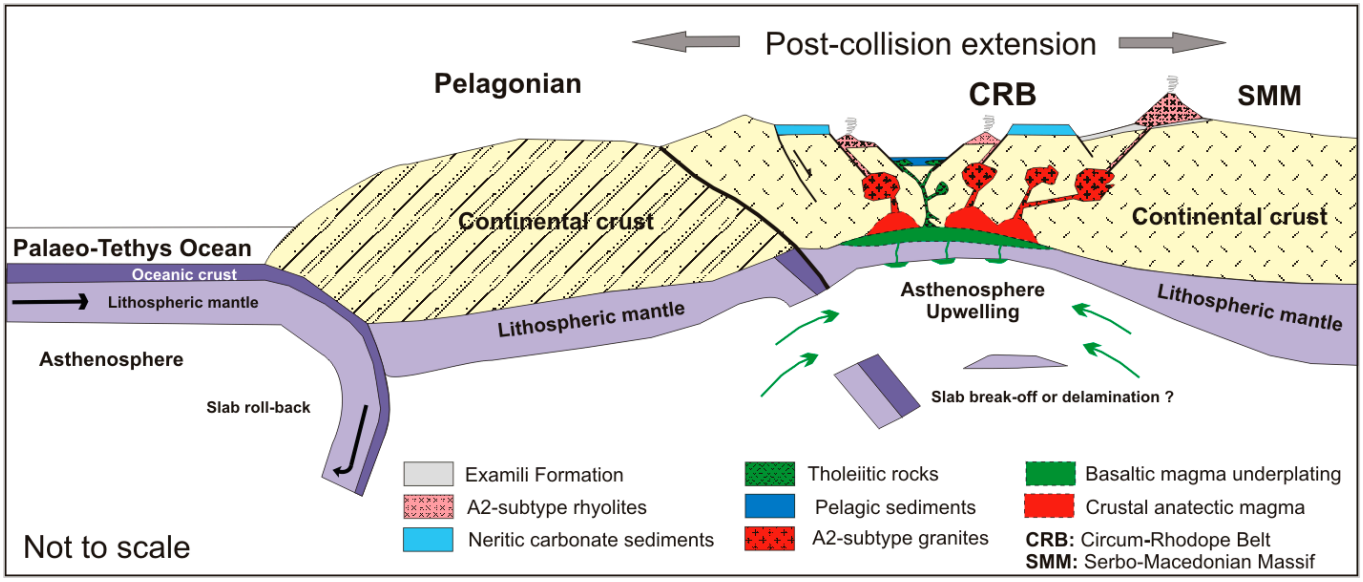

Figure 23. Schematic diagram illustrating the petrogenetic model for the generation of the Permo–Triassic bimodal volcanism [rhyolite (crustal melts)—basalt (mantle melts)] during a post-collision extensional stage of the Variscan continental crust (the SMM–Vertiskos and Pelagonian terranes). The A2-subtype rhyolites from the CRB, the tholeiitic basalts and dolerites from the Akritas–Metallikon area, and the A2-subtype Arnea and Kerkini granites are shown.

According to previous studies, this Permo–Triassic bimodal magmatism (including plutonic and volcanic rocks) is linked to the early extensional rifting stage that separated the Vertiskos and the Pelagonian terranes, eventually leading to the opening of the Mesozoic Meliata/Maliac–Vardar/Axios Ocean (e.g., [12,13,17,19,20,39,40,42,43,81]). Mposkos et al. [81] correlate the Triassic intrusion of the Arnea–Kerkini granites and the Volvi metagabbro with the second low-pressure, high-temperature (LP–HT) metamorphic event in the Vertiskos Unit and the subsequent formation of the East-Vardar basin. This study suggests that magma generation of the CRB silicic volcanic rocks occurred under similar conditions,

which are likely associated with the Triassic LP–HT metamorphic event in the Vertiskos Unit.

The geochemical study of the Permo–Triassic CRB silicic volcanic rocks presented in this paper, supported by updated literature, reveals that they are peraluminous, crust-derived, A2-subtype granitoids. Their genesis is most likely related to the post-collisional extension of the Variscan crystalline basement (Vertiskos Unit) rather than anorogenic within-plate continental rifting. This inference aligns with the suggestion of Poli et al. [18,41] regarding the formation of their plutonic equivalents, the Arnea and Kerkini A2-subtype granites, in an incipient rift environment after continental collision where the continental crust was still present. The Permo–Triassic age and post-collisional nature of this silicic magmatism (the CRB silicic volcanic rocks and Arnea–Kerkini granites), along with its origin from the partial melting of the Vertiskos Unit basement crustal rocks (metapelites), as well as its association with the mantle-derived basic tholeiitic rocks from the Akritas–Metallikon area, provide new constraints on the geodynamic evolution of the broader region.

6.6. Geodynamic Implications

The Permo–Triassic post-collisional bimodal volcanism (A-type rhyolites and tholeiitic basalts) in the CRB is an integral part of a larger system that delineates the borders of the Serbo-Macedonian (Vertiskos Unit) and the Pelagonian continental fragments as indicated in Figure 24.

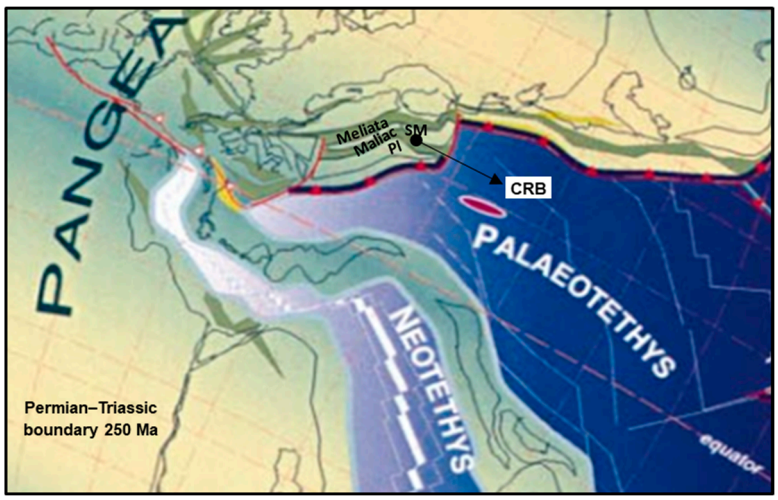

Figure 24. Schematic paleogeographic map during the Permian–Triassic boundary (modified from [2]). The dark green areas are initial "rift" or "back arc" basins (e.g., Meliata, Maliac). The inferred position of the post-collisional CRB silicic volcanism, investigated in this paper, is indicated with the black dot. SM: Serbo-Macedonian and Pl: Pelagonian continental blocks.

During the Late Carboniferous, the Variscan lithosphere was overthickening due to the imbrication and amalgamation of the different blocks of Gondwanan origin (the Vertiskos Unit of SMM and the Pelagonian, among them) to Eurasia and slab detachment of the intervening oceans (e.g., [3,4,6]). The syn-collisional S-type meta-granites of Polydendri [77] and Theodorio [78] emplaced into the Vertiskos Unit are likely associated with the Late Carboniferous to early Permian collision-related magmatism that resulted from these events [6,76]. The amalgamation of the blocks was quickly followed by lithospheric collapse above the retreating Palaeo-Tethys slab, spanning from Sicily to the Middle East [6]. Large volumes of Carboniferous–Permian intrusive rocks in the Pelagonian terrane are associated with prolonged subduction of the Palaeo-Tethys to the north under the Eurasian

margin [202,203]. The transition from collision and compression to the post-collisional extension stage of the Variscan continental lithosphere is marked by a shift from arc-related calc-alkaline plutonic activity in the Late Carboniferous–Early Permian to K-alkaline silicic magmatism of Late Permian–Early Triassic age [3,4,6].

Post-collisional granitoids typically formed shortly after the subduction and collision of tectonic plates. The magmatic activity is completed within a relatively short time span and is often associated with ophiolite belts or suture zones [105]. In North Macedonia, the Galicia–Moldanubian Ocean, an oceanic domain that separated the SMM in the east and the Pelagonian Massif in the west, was finally closed due to subduction. This was followed by the amalgamation of Pelagonian with SMM, leading to the thickening of the Variscan lithosphere ([204,205] and references therein). In Greece, there is no clear or unequivocal evidence of a collision between the Vertiskos and the Pelagonian continental blocks prior to the Triassic rifting that separated them. However, the extensive amphibolites occurring in the Vertiskos Unit (a few of them are recognized as ex-eclogites [77,78,81]) may represent remnants of oceanic crust involved in pre-Triassic subduction, obduction, and collision processes, potentially indicating an exposed suture zone [19]. Recent U–Pb zircon dating (LA-ICP-MS) of amphibolites reveals metamorphic ages of 341 Ma and 319–321 Ma [20,80], implying a pre-Carboniferous protolith for them. These ages likely correspond to the first HP–HT metamorphic Carboniferous event in the Vertiskos Unit, which is indicative of the Variscan subduction and collision processes [81].

In summary, from the Late Permian to Early Triassic, the rollback of the Palaeo-Tethyan slab caused the collapse of large portions of the European Variscan orogen. Several Permian rifts formed due to extension, and some developed into back-arc basins (e.g., Meliata, Maliac) during the Triassic (e.g., [2–6]). The Permo–Triassic A2-subtype CRB silicic volcanic rocks examined in this study, along with the associated Arnea and Kerkini granites, most likely originated from the partial melting of ancient crustal pelitic rocks of the Vertiskos Unit under low-pressure, high-temperature (LP–HT) conditions in a post-collision extensional tectonic regime. A contribution of basaltic material from the asthenosphere supported this process, primarily as a heat source. Their genesis is consistent with the breakup of the Pangea supercontinent in the Permian–Triassic period, the subsequent opening of the Mesozoic Neo-Tethyan Maliac/Vardar Ocean, and the detachment of Pelagonian from the Vertiskos (SMM) terrane.

The identification of this post-collisional A2-subtype silicic magmatism (the CRB silicic volcanic rocks and the Arnea and Kerkini granites) at the Permian–Triassic boundary confirms the continental collision between the Vertiskos (SMM) and Pelagonian microcontinents in the Variscan orogen and indicates that the peak collision between these Gondwana-derived terranes must have been completed by at least the earliest Late Permian.

7. Conclusions

The investigation of whole-rock geochemistry of the Permo–Triassic silicic volcanic rocks from the Circum-Rhodope Belt (CRB) in northern Greece provides new insights into their petrogenesis and the geodynamic evolution of the broader region. The concluding remarks are as follows:

- The CRB silicic volcanic rocks are peraluminous, subalkaline, A2-subtype granitoids characterized by relative enrichment in K, Rb, Th, Zr, Y, and Pb and depletion in Nb, Ba, Sr, P, and Ti.
- They have markedly high Y/Nb (average = 3.36), Rb/Sr (average = 15.8), and Rb/Nb (average = 16.2) ratios, suggesting crustal magma sources derivation and emplacement in a post-collisional environment.

- The rocks have a low CaO/Na_2O ratio (<0.5) consistent with pelite-derived magmas and a low Al_2O_3/TiO_2 ratio (<100), indicating high-temperature melting, which is consistent with their high zircon saturation temperatures (T_{Zr} > 800 °C).
- Their higher normative Or, relative to An and Ab contents, and their low Pb/Ba ratio (average = 0.06) indicate derivation from biotite dehydration melting.
- They have a very low Sr/Y ratio (average = 0.37), and a higher Rb/Sr ratio compared to the Vertiskos metapelites (likely parent rocks), suggesting the presence of plagioclase but little or no garnet in the source residue. This residual phase indicates relatively low pressures (0.4–0.8 GPa) and shallow to moderate depths (15–30 km) of magma origin.
- The partial melting of the Vertiskos lower crust is attributed to conductive heating caused by magmatic underplating resulting from asthenosphere upwelling. This process later led to the extrusion of minor Triassic tholeiitic basalts and dolerites, indicating that the Triassic volcanism was bimodal.
- In northern Greece, the occurrence of these unique post-collisional bimodal volcanic rocks (A2-subtype rhyolites and minor tholeiitic basalts), along with the associated Arnea and Kerkini granites, indicates that the area experienced a tectonic transition from compression to extension at the Permian–Triassic boundary, marking the initial stage in the development of the Maliac–Vardar Ocean. This strongly suggests that the final amalgamation of the Pelagonian and Vertiskos terranes had been completed by the earliest Late Permian.

Supplementary Materials: The following supporting information can be downloaded at https://www.mdpi.com/article/10.3390/geosciences15020048/s1, Table S1: Representative X-ray fluorescence (XRF) major and trace element analyses, calculated CIPW norms, some elemental ratios, and zircon saturation temperatures (T_{Zr}) of the CRB silicic volcanic rocks (files: Akritas, Metallikon, Nea Santa, Kolchida, and Sana).

Funding: This research received no external funding.

Data Availability Statement: Data is contained within the Supplementary Material.

Acknowledgments: I would like to extend my sincere thanks to Emeritus Professor Sarantis Dimitriadis for sharing his knowledge of these "unique" rocks and for the insightful discussions we had. I further acknowledge three anonymous reviewers for their constructive comments and suggestions.

Conflicts of Interest: The author declares no conflicts of interest.

References

1. Brunn, J.H. Contribution à l'étude géologique du Pinde septentrional et d'une partie de la Macédoine occidentale. *Ann. Géol. Pays Héll.* **1956**, *7*, 1–358.
2. Stampfli, G.M.; Borel, G.D. A plate tectonic model for the Paleozoic and Mesozoic constrained by dynamic plate boundaries and restored synthetic oceanic isochrons. *Earth Planet. Sci. Lett.* **2002**, *196*, 17–33. [CrossRef]
3. Stampfli, G.M.; von Raumer, J.F.; Borel, G.D. Paleozoic evolution of pre-Variscan terranes: From Gondwana to the Variscan collision. In *Variscan-Appalachian Dynamics: The Building of the Late Paleozoic Basement*; Special Paper 364; Geological Society of America: Boulder, CO, USA, 2002; pp. 263–280.
4. Stampfli, G.M.; Kozur, H.W. Europe from the Variscan to the Alpine cycles. In *European Lithosphere Dynamics*; Gee, D.G., Stephenson, R.A., Eds.; Geological Society of London Memoirs; Geological Society of London: London, UK, 2006; Volume 32, pp. 57–82. [CrossRef]
5. Stampfli, G.M.; Hochard, C. Plate tectonics of the Alpine realm. In *Ancient Orogens and Modern Analogues*; Murphy, J.B., Keppie, J.D., Hynes, A.J., Eds.; Geological Society, London, Special Publications: London, UK, 2009; Volume 327, pp. 89–111. [CrossRef]
6. Stampfli, G.M.; Hochard, C.; Vérard, C.; Wilhem, C.; von Raumer, J. The formation of Pangea. *Tectonophysics* **2013**, *593*, 1–19. [CrossRef]

7. Spahić, D. Elusive Permian-Triassic Western Paleotethyan paleogeography: Towards the Early Cimmerian pre-Vardar configuration (Dinarides-Carpathian Balkan Belt). *Earth-Sci. Rev.* **2024**, *256*, 104857. [CrossRef]
8. Pe-Piper, G.; Piper, D.J.W. *The Igneous Rocks of Greece. The Anatomy of an Orogen*; Gebruder Borntraeger: Berlin, Germany; Stuttgart, Germany, 2002; pp. 1–645.
9. Robertson, A.H.F. Overview of the genesis and emplacement of Mesozoic ophiolites in the Eastern Mediterranean Tethyan region. *Lithos* **2002**, *65*, 1–67. [CrossRef]
10. Papanikolaou, D. Timing of tectonic emplacement of the ophiolites and terrane paleogeography in the Hellenides. *Lithos* **2009**, *108*, 262–280. [CrossRef]
11. Rassios, A.E.; Smith, A.; Kostopoulos, D. Ophiolites 2008 Guidebook: Link between the Mesohellenic Ophiolites and the Pelagonian Margin. *J. Virtual Explor.* **2009**, *34*, 57. [CrossRef]
12. Ferriere, J.; Baumgartner, P.O.; Chanier, F. The Maliac Ocean: The origin of the Tethyan Hellenic ophiolites. *Int. J. Earth Sci. (Geol. Rundsch.)* **2016**, *105*, 1941–1963. [CrossRef]
13. Kilias, A. The Alpine Geological History of the Hellenides from the Triassic to the Present–Compression vs. Extension, a Dynamic Pair for Orogen Structural Configuration: A Synthesis. *Geosciences* **2024**, *14*, 10. [CrossRef]
14. Vergély, P.; Mercier, J.L. An overview of the evolution of the internal hellenides (Albania, Republic of North Macedonia, Greek Central Macedonia): Obductions, collisions and North Aegean extension. *BSGF-Earth Sci. Bull.* **2024**, *195*, 9. [CrossRef]
15. Mountrakis, D.; Eleftheriadis, G.; Christofides, G.; Kilias, A.; Sapountzis, E. Silicic Metavolcanics in the Western Pelagonian Margin of Greece Related to the Opening of Neo-Tethys. *Chem. Erde* **1987**, *47*, 167–180.
16. Asvesta, A. Magmatism and Associated Sedimentation During the First Stage of the Opening of the Vardar Oceanic Basin in Triassic Times. Ph.D. Thesis, University of Thessaloniki, Thessaloniki, Greece, 1992; 439p. (In Greek, with English Summary)
17. Christofides, G.; Koroneos, A.; Liati, A.; Kral, J. The A-type Kerkini granitic complex in north Greece: Geochronology and geodynamic implications. *Bull. Geol. Soc. Greece* **2007**, *40*, 700–711. [CrossRef]
18. Poli, G.; Christofides, G.; Koroneos, A.; Soldatos, T.; Perugini, D.; Langone, A. Early triassic granitic magmatism—Arnea and Kerkini granitic complexes—In the Vertiskos unit (Serbo-macedonian massif, north-eastern Greece) and its significance in the geodynamic evolution of the area. *Acta Vulcanol.* **2009**, *21*, 47–70.
19. Asvesta, A.; Dimitriadis, S. Facies architecture of a Triassic rift-related Silicic Volcano-Sedimentary succession in the Tethyan realm, Peonias subzone, Vardar (Axios) Zone, northern Greece. *J. Volcanol. Geotherm. Res.* **2010**, *193*, 245–269. [CrossRef]
20. Bonev, N.; Moritz, R.; Borisova, M.; Filipov, P. Therma-Volvi-Gomati complex of the Serbo-Macedonian Massif, Northern Greece: A Middle Triassic continental margin ophiolite of Neotethyan origin. *J. Geol. Soc.* **2019**, *176*, 931–944. [CrossRef]
21. Pamić, J.; Balen, D. Interaction between Permo-Triassic rifting, magmatism and initiation of the Adriatic–Dinaridic carbonate platform (ADCP). *Acta Geol. Hung.* **2005**, *48*, 181–204. [CrossRef]
22. Bonev, N.; Filipov, P.; Raicheva, R.; Moritz, R. Triassic magmatism along the Maritsa river valley, Sakar-Strandzha Zone, Bulgaria. *Rev. Bulg. Geol. Soc.* **2019**, *80*, 56–57.
23. Ondrejka, M.; Uher, P.; Putiš, M.; Kohút, M.; Broska, I.; Larionov, A.; Bojar, A.-V.; Sobocký, T. Permian A-type granites of the Western Carpathians and Transdanubian regions: Products of the Pangea supercontinent breakup. *Int. J. Earth Sci.* **2021**, *110*, 2133–2155. [CrossRef]
24. Georgiev, S.; Lazarova, A.; Balkanska, E. Permian–Triassic A-type rhyolites from the Central Balkanides (Stara Planina Mountains), Bulgaria. *Rev. Bulg. Geol. Soc.* **2022**, *83*, 77–80. [CrossRef]
25. Aysal, N.; Şahin, S.Y.; Güngör, Y.; Peytcheva, I.; Öngen, S. Middle Permian–early Triassic magmatism in the Western Pontides, NW Turkey: Geodynamic significance for the evolution of the Paleo-Tethys. *J. Asian Earth Sci.* **2018**, *164*, 83–103. [CrossRef]
26. Akal, C.; Candan, O.; Koralay, O.E.; Gerdes, A.; Oberhaensli, R. Middle triassic magmatism in the Afyon Zone of the Anatolides/Eastern Mediterranean: Implications for the extension of the Northern margin of Gondwana and opening of the Inner-Tauride Ocean. *Lithos* **2024**, *482–483*, 107691. [CrossRef]
27. Whalen, J.B.; Currie, K.I.; Chappell, B.W. A-type granites: Geochemical characteristic, discrimination and petrogenesis. *Contrib. Mineral. Petrol.* **1987**, *95*, 407–419. [CrossRef]
28. Hildreth, W.; Halliday, A.N.; Christiansen, R.L. Isotopic and chemical evidence concerning the genesis and contamination of basaltic and rhyolitic magma beneath the Yellowstone plateau volcanic field. *J. Petrol.* **1991**, *32*, 63–138. [CrossRef]
29. Eby, G.N. Chemical subdivision of the A-type granitoids: Petrogenetic and tectonic implications. *Geology* **1992**, *20*, 641–644. [CrossRef]
30. Turner, S.; Sandiford, M.; Foden, J. Some geodynamic and compositional constraints on "postorogenic" magmatism. *Geology* **1992**, *20*, 931–934. [CrossRef]
31. Frost, C.D.; Frost, B.R. Reduced rapakivi-type granites: The tholeiite connection. *Geology* **1997**, *25*, 647–650. [CrossRef]
32. Frost, C.D.; Frost, B.R.; Chamberlain, K.R.; Edwards, B.R. Petrogenesis of the 1.43 Ga Sherman batholith, SE Wyoming, USA: A reduced, rapakivi-type anorogenic granite. *J. Petrol.* **1999**, *40*, 1771–1802. [CrossRef]

33. Frost, C.D.; Bell, J.M.; Frost, B.R.; Chamberlain, K.R. Crustal growth by magmatic underplating: Isotopic evidence from the northern Sherman batholith. *Geology* **2001**, *29*, 515–518. [CrossRef]
34. Bonin, B. Do coeval mafic and felsic magmas in post-collisional to within-plate regimes necessarily imply two contrasting, mantle and crustal, sources? A review. *Lithos* **2004**, *78*, 1–24. [CrossRef]
35. Bonin, B. A-type granites and related rocks: Evolution of a concept, problems and prospects. *Lithos* **2007**, *97*, 1–29. [CrossRef]
36. Zhang, X.H.; Zhang, H.F.; Tang, Y.J.; Wilde, S.A.; Hu, Z.C. Geochemistry of Permian bimodal volcanic rocks from central Inner Mongolia, North China: Implication for tectonic setting and Phanerozoic continental growth in Central Asian Orogenic Belt. *Chem. Geol.* **2008**, *249*, 262–281. [CrossRef]
37. Christofides, G.; Koroneos, A.; Pe-Piper, G.; Katirtzoglou, K.; Chatzikiriakou, A. Pre-tertiary A-type magmatism in the Serbo-macedonian massif (N. Greece): Kerkini granitic complex. *Bull. Geol. Soc. Greece* **1999**, *33*, 131–148.
38. Christofides, G.; Koroneos, A.; Soldatos, T.; Eleftheriadis, G. Mesozoic magmatism in the area between the Vardar (Axios) zone and the Serbo-macedonian masiff (northern Greece). In Proceedings of the International Symposium on Geology and Metallogeny of the Dinarides and the Vardar Zone, Banja Luka, Bosnia and Herzegovina, 3–6 October 2000; pp. 111–120.
39. Christofides, G.; Koroneos, A.; Liati, A.; Kral, J. Geochronology of the Kerkini granitic complex (Serbomacedonian massif, N. Greece) and geodynamic implications. In Proceedings of the XVIIIth Congress of the Carpathian-Balkan Geological Association, Belgrade, Serbia, 3–6 September 2006; pp. 61–64.
40. Himmerkus, F.; Reischmann, T.; Kostopoulos, D. Triassic rift related meta-granites in the Internal Hellenides, Greece. *Geol. Mag.* **2009**, *146*, 252–265. [CrossRef]
41. Poli, G.; Christofides, G.; Koroneos, A. A-type granites in the Internal Hellenides (Macedonia, Greece): Rift-related or post-orogenic? A reappraisal. *Geophys. Res. Abs.* **2010**, *12*, EGU2010-4043.
42. Ferrière, J.; Stais, A. Nouvelle interprétation de la suture téthysienne vardarienne d'après l'analyse des séries de Péonias (Vardar oriental, Hellénides internes). (New interpretation of the Vardarian Tethysian area based on the Peonian series). *Bull. Soc. Géol. Fr.* **1995**, *166*, 327–339. [CrossRef]
43. Dimitriadis, S.; Asvesta, A. Sedimentation and magmatism related to the Triassic rifting and later events in the Vardar-Axios zone. *Bull. Geol. Soc. Greece* **1993**, *28*, 149–168.
44. Asvesta, A.; Dimitriadis, S. Magma-sediment interaction during the emplacement of syn-sedimentary silicic and mafic intrusions and lavas into and onto Triassic strata (Circum-Rhodope Belt, northern Greece). *Geol. Carpathica* **2013**, *64*, 181–194. [CrossRef]
45. Asvesta, A.; Dimitriadis, S. Geochemical characteristics and Tectonic significance of Permo-Triassic Silicic Volcanic rocks from Circum-Rhodope Belt, Vardar (Axios) Zone, northern Greece. In Proceedings of the 15th International Congress of the Geological Society of Greece, Athens, Greece, 22–24 May 2019; pp. 307–308.
46. Asvesta, A.; Dimitriadis, S. Triassic Basic and Intermediate Rift-related Volcanic Rocks from Akritas-Metallikon area, Circum-Rhodope Belt, northern Greece. In Proceedings of the 16th International Congress of the Geological Society of Greece, Patras, Greece, 17–19 October 2022.
47. Stais, A.; Ferrière, J. Nouvelles donnees sur la paleogeographie Mesozoique du domaine Vardarien: Les bassins d'Almopias et de Peonias (Macédoine, Hellenides Internes Septentrionales). *Bull. Geol. Soc. Greece* **1991**, *25*, 491–507.
48. Asvesta, A.; Dimitriadis, S. The Nea Santa submarine rhyolite dome of the Triassic Silicic Volcano-Sedimentary succession, Circum-Rhodope Belt, northern Greece. In Proceedings of the Geologica Balcanica, XIX Congress of the Carpathian-Balkan Geological Association, Thessaloniki, Greece, 23–26 September 2010; Abstracts Volume 39, pp. 30–31.
49. Mercier, J. 1966/68. I—Études géologique des zones internes des Hellénides en Macédoine Centrale (Grèce). II—Contribution à l'étude du métamorphisme et de l'évolution magmatiques des zones internes des Hellénides. Thèse Doct. Ès Sciences, Univ. Paris. *Ann. Géol. Pays Hell.* **1975**, *20*, 1–792.
50. Jacobshagen, V. *Geologie von Griechenland. Beiträge zur Regionalen Geologie der Erde, Band 19*; Gebrüder Bornträger: Berlin, Germany, 1986; p. 363.
51. Robertson, A.H.F.; Dixon, J.E. Introduction: Aspects of the geological evolution of the Eastern Mediterranean. In *The Geological Evolution of the Eastern Mediterranean*; Dixon, J.E., Robertson, A.H.F., Eds.; Geological Society: London, UK; Special Publications: London, UK, 1984; Volume 17, pp. 1–74.
52. Haenel-Remy, S.; Bébien, J. The Oreokastro Ophiolite (Greek Macedonia): An important component of the Innermost Hellenic Ophiolite Belt. *Ofioliti* **1985**, *10*, 279–296.
53. Bébien, J.; Dubois, R.; Gauthier, A. Example of ensialic ophiolites emplaced in a wrench zone: Innermost Hellenic ophiolite belt (Greek Macedonia). *Geology* **1986**, *14*, 1016–1019. [CrossRef]
54. Bébien, J.; Baroz, J.; Caperdi, S.; Venturelli, G. Magmatisme basique associées à l'ouverture d'un basin marginal dans les Héllenides internes au Jurassic. *Ofioliti* **1987**, *12*, 53–70.
55. Robertson, A.H.F.; Clift, P.D.; Degnan, D.J.; Jones, G. Palaeogeographic and palaeotectonic evolution of the eastern Mediterranean Neotethys. *Palaeogeogr. Palaeoclimatol. Palaeoecol.* **1991**, *87*, 289–343. [CrossRef]

56. Sharp, I.; Robertson, A.H.F. Tectonic-sedimentary evolution of the western margin of the Mesozoic Vardar Ocean: Evidence from the Pelagonian and Almopias zones, northern Greece. In *Tectonic Development of the Eastern Mediterranean Region*; Robertson, A.H.F., Mountrakis, D., Eds.; Geological Society: London, UK; Special Publications: London, UK, 2006; Volume 260, pp. 373–412. [CrossRef]
57. Zachariadis, P.T. Ophiolites of the Eastern Vardar Zone, N. Greece. Ph.D. Thesis, Johannes Gutenberg-Universität, Mainz, Germany, 2007; 221p.
58. Saccani, E.; Beccaluva, L.; Photiades, A.; Zeda, O. Petrogenesis and tectono-magmatic significance of basalts and mantle peridotites from the Albanian–Greek ophiolites and sub-ophiolitic mélanges. New constraints for the Triassic–Jurassic evolution of the Neo-Tethys in the Dinaride sector. *Lithos* **2011**, *124*, 227–242. [CrossRef]
59. Ferrière, J. Étude géologique d'un sectuer des zones Helléniques internes subpelagonienne et pélagonienne (massif de l'Othrys, Grèce continental). Importance et signification de l période orogénique ante-Cretacé superieur. *Bull. Soc. Géol. Fr.* **1974**, *7*, 543–562. [CrossRef]
60. Mountrakis, D. The Pelagonian Zone in Greece: A Polyphase-Deformed Fragment of the Cimmerian Continent and Its Role in the Geotectonic Evolution of the Eastern Mediterranean. *J. Geol.* **1986**, *94*, 335–347. [CrossRef]
61. Robertson, A.H.F.; Dixon, J.E.; Brown, S.; Collins, A.; Morris, A.; Pickett, E.; Sharp, I.; Ustaömer, T. Alternative tectonic models for the Late Palaeozoic-Early Tertiary development of Tethys in the Eastern Mediterranean region. *Geol. Soc. Lond. Spec. Publ.* **1996**, *105*, 239–263. [CrossRef]
62. Robertson, A.; Karamata, S.; Šarić, K. Overview of ophiolites and related units in the Late Palaeozoic–Early Cenozoic magmatic and tectonic development of Tethys in the northern part of the Balkan region. *Lithos* **2009**, *108*, 1–36. [CrossRef]
63. Robertson, A.H. Late Palaeozoic–Cenozoic tectonic development of Greece and Albania in the context of alternative reconstructions of Tethys in the Eastern Mediterranean region. *Int. Geol. Rev.* **2013**, *54*, 373–454. [CrossRef]
64. Papanikolaou, D. Tectonostratigraphic models of the Alpine terranes and subduction history of the Hellenides. *Tectonophysics* **2013**, *595–596*, 1–24. [CrossRef]
65. Kilias, A.; Tranos, M.; Mountrakis, D.; Shallo, M.; Marto, A.; Turku, I. Geometry and kinematics of deformation in the Albanian orogenic belt during the Tertiary. *J. Geodyn.* **2001**, *31*, 169–187. [CrossRef]
66. Gawlick, H.-J.; Frisch, W.; Hoxha, L.; Dumitrica, P.; Krystyn, L.; Lein, R.; Missoni, S.; Schlagintweit, F. Mirdita Zone ophiolites and associated sediments in Albania reveal Neotethys Ocean origin. *Int. J. Earth Sci.* **2008**, *97*, 865–881. [CrossRef]
67. Kilias, A.; Frisch, W.; Avgerinas, A.; Dunkl, I.; Falalakis, G.; Gawlick, H.-J. Alpine architecture and kinematics of de-formation of the northern Pelagonian nappe pile in the Hellenides. *Austrian J. Earth Sci.* **2010**, *103*, 4–28. [CrossRef]
68. Ferrière, J.; Chanier, F.; Ditbanjong, P. The Hellenic ophiolites: Eastward or westward obduction of the Maliac Ocean, a discussion. *Int. J. Earth Sci.* **2012**, *101*, 1559–1580. [CrossRef]
69. Bortolotti, V.; Chiari, M.; Marroni, M.; Pandolfi, L.; Principi, G.; Saccani, E. Geodynamic evolution of ophiolites from Albania and Greece (Dinaric-Hellenic belt): One, two, or more oceanic basins? *Int. J. Earth Sci. (Geol. Rundsch.)* **2013**, *102*, 783–811. [CrossRef]
70. Froitzheim, N.; Jahn-Awe, S.; Frei, D.; Wainwright, A.N.; Maas, R.; Georgiev, N.; Nagel, T.J.; Pleuger, J. Age and composition of meta-ophiolite from the Rhodope Middle Allochthon (Satovcha, Bulgaria): A test for the maximum-allochthony hypothesis of the Hellenides. *Tectonics* **2014**, *33*, 1477–1500. [CrossRef]
71. Schenker, F.L.; Burg, J.; Kostopoulos, D.; Moulas, E.; Larionov, A.; von Quadt, A. From Mesoproterozoic magmatism to collisional Cretaceous anatexis: Tectonomagmatic history of the Pelagonian Zone, Greece. *Tectonics* **2014**, *33*, 1552–1576. [CrossRef]
72. Kockel, F.; Mollat, H.; Walther, H.W. Geologie des Serbo-Mazedonischen Massivs und seines Mesozoischen rahmens (Nord Griechenland). *Geol. Jb.* **1971**, *89*, 529–551.
73. Kockel, F.; Mollat, H.; Walther, H.W. *Erläuterungen zur Geologischen Karte der Chalkidhiki und angrenzender Gebiete 1:100000, (Nord-Griechenland)*; Bundesanstalt fur Geowissenschaften und Rohstoffe: Hannover, Germany, 1977; 119p.
74. Himmerkus, F.; Anders, B.; Reischmann, T.; Kostopoulos, D. Gondwana-derived terranes in the northern Hellenides. In *4-D Framework of Continental Crust*; Hatcher, R.D., Jr., Carlson, M.P., McBride, J.H., Martínez Catalán, J.R., Eds.; Geological Society of America Memoir; Geological Society of America: Boulder, CO, USA, 2007; Volume 200, pp. 379–390. [CrossRef]
75. Himmerkus, F.; Reischmann, T.; Kostopoulos, D. Serbo-Macedonian revisited: A Silurian basement terrane from northern Gondwana in the Internal Hellenides, Greece. *Tectonophysics* **2009**, *473*, 20–35. [CrossRef]
76. Antić, M.; Peytcheva, I.; von Quadt, A.; Kounov, A.; Trivić, B.; Serafimovski, T.; Tasev, G.; Gerdjikov, I.; Wetzel, A. Pre-Alpine evolution of a segment of the North-Gondwanan margin: Geochronological and geochemical evidence from the central Serbo-Macedonian Massif. *Gondwana Res.* **2016**, *36*, 523–544. [CrossRef]
77. Kourou, A. Lithology, Geochemistry, Tectonics and Metamorphism of a Part of the Western Vertiscos Group. The Area Northeast of Lake Koroneia. Ph.D. Thesis, University of Thessaloniki, Thessaloniki, Greece, 1991; 461p. (In Greek, with English Summary)
78. Sidiropoulos, N. Lithology, Geochemistry, Tectonics and Metamorphism of the Northwestern Part of the Vertiscos Group. The Area of Mount Dysoro (Krousia) North of Kilkis. Ph.D. Thesis, University of Thessaloniki, Thessaloniki, Greece, 1991; 592p. (In Greek, with English Summary)

79. Dixon, J.E.; Dimitriadis, S. The metamorphic evolution of the Serbo-Macedonian Massif in Greece. In *4th EUG Meeting Strasburg*; Terra Cognita: Helsinki, Finland, 1987; Volume 7, p. 107.
80. Kydonakis, K.; Brun, J.-P.; Sokoutis, D.; Gueydan, F. Kinematics of Cretaceous subduction and exhumation in the western Rhodope (Chalkidiki block). *Tectonophysics* **2015**, *665*, 218–235. [CrossRef]
81. Mposkos, E.; Krohe, A.; Baziotis, I. Deep tectonics in the eastern hellenides uncovered: The record of Variscan continental amalgamation, Permo-Triassic rifting, and early Alpine Collision in pre-Variscan continental crust in the W-Rhodope (Vertiscos-Ograzden Complex, N-Greece). *Tectonics* **2021**, *40*, e2019TC005557. [CrossRef]
82. Kostopoulos, D.; Reischemann, T.; Sklavounos, S. Palaeozoic and Early Mesozoic Magmatism and Metamorphism in the Serbo-Macedonian Massif, Central Macedonia, Northern Greece. In *Symposium: Integrated Tectonic Studies of the Evolution of the Tethyan Orogenic Belt in the Eastern Mediterranean Region*; LS03 The Evolution of the Tethyan Orogenic Belt, Abstracts; AGU: Strasbourg, France, 2001; Volume 11, p. 318.
83. Kockel, F.; Ioannides, K. *Kilkis Sheet, 1:50000 Geological Map of Greece*; IGME's Geoscientific Information: Athens, Greece, 1979.
84. Meinhold, G.; Kostopoulos, D.K. The Circum-Rhodope Belt, northern Greece: Age, provenance, and tectonic setting. *Tectonophysics* **2013**, *595–596*, 55–68. [CrossRef]
85. Meinhold, G.; Kostopoulos, D.; Reischmann, T.; Frei, D.; BouDagher-Fadel, M.K. Geochemistry, provenance and stratigraphic age of metasedimentary rocks from the eastern Vardar suture zone, northern Greece. *Palaeogeogr. Palaeoclimatol. Palaeoecol.* **2009**, *277*, 199–225. [CrossRef]
86. Kauffmann, G.; Kockel, F.; Mollat, H. Notes on the stratigraphic and paleogeographic position of the Svoula Formation in the Innermost Zone of the Hellenides (Northern Greece). *Bull. Soc. Géol. Fr.* **1976**, *18*, 225–230. [CrossRef]
87. Kockel, F. Die Vardar–(Axios) Zone. In *Geologie von Griechenland*; Jacobshagen, V., Ed.; Gebrüder Borntraeger: Berlin, Germany; Stuttgart, Germany, 1986; pp. 150–168.
88. Kauffmann, G. Perm und Trias im östlichen Mittelgriechenland und auf einigen ägäischen inseln. *Z. Dtsch. Geol. Ges.* **1976**, *127*, 387–398.
89. Pearce, J.A.; Cann, J.R. Tectonic setting of basic volcanic rocks determined using trace element analyses. *Earth Planet. Sci. Lett.* **1973**, *19*, 290–300. [CrossRef]
90. Pearce, J.A. Trace element characteristics of lavas from destructive plate boundaries. In *Andesites*; Thorpe, R.S., Ed.; J. Wiley & Sons: Hoboken, NJ, USA, 1982; pp. 525–548.
91. Winchester, J.A.; Floyd, P.A. Geochemical discrimination of different magma series and their differentiation products using immobile elements. *Chem. Geol.* **1977**, *20*, 325–343. [CrossRef]
92. Irvine, T.N.; Baragar, W.P.A. A guide to the chemical classification of common volcanic rocks. *Can. J. Earth Sci.* **1971**, *8*, 523–548. [CrossRef]
93. Maniar, P.D.; Piccoli, P.M. Tectonic discrimination of granitoids. *Geol. Soc. Am. Bull.* **1989**, *101*, 635–643. [CrossRef]
94. Frost, B.R.; Barnes, C.G.; Collins, W.J.; Arculus, R.J.; Ellis, D.J.; Frost, C.D. A geochemical classification for granitic rocks. *J. Petrol.* **2001**, *42*, 2033–2048. [CrossRef]
95. Sylvester, P.J. Post-Collisional Strongly Peraluminous Granites. *Lithos* **1998**, *45*, 29–44. [CrossRef]
96. Kong, H.; Li, H.; Wu, Q.-H.; Xi, X.-S.; Dick, J.M.; Gabo-Ratio, J.A.S. Co-development of Jurassic I-type and A-type granites in southern Hunan, South China: Dual control by plate subduction and intraplate mantle upwelling. *Chem. Erde* **2018**, *78*, 500–520. [CrossRef]
97. King, P.L.; White, A.J.R.; Chappell, B.W.; Allen, C.M. Characterization and origin of aluminous A-type granites from the Lachlan Fold Belt, southeastern Australia. *J. Petrol.* **1997**, *38*, 371–391. [CrossRef]
98. Sun, S.-S.; McDonough, W.F. Chemical and isotopic systematics of ocean basalts: Implications for mantle composition and processes. In *Magmatism in Ocean Basins*; Saunders, A.D., Norry, M.J., Eds.; Geological Society: London, UK; Special Publications: London, UK, 1989; Volume 42, pp. 313–345. [CrossRef]
99. Loiselle, M.C.; Wones, D.R. Characteristics and origin of anorogenic granites. *Geol. Soc. Am.* **1979**, *11*, 468.
100. Chappell, B.W.; White, A.J.R. Two contrasting granite types. *Pac. Geol.* **1974**, *8*, 173–174.
101. Eby, G.N. The A-type granitoids: A review of their occurrence and chemical characteristics and speculations on their petrogenesis. *Lithos* **1990**, *26*, 115–134. [CrossRef]
102. Frost, C.D.; Frost, B.R. On Ferroan (A-type) Granitoids: Their Compositional Variability and Modes of Origin. *J. Petrol.* **2011**, *52*, 39–53. [CrossRef]
103. Clemens, J.D. S-type granitic magmas–petrogenetic issues, models and evidence. *Earth-Sci. Rev.* **2003**, *61*, 1–18. [CrossRef]
104. Collins, W.J.; Beams, S.D.; White, A.J.R.; Chappell, B.W. Nature and origin of A-type granites with particular reference to southeastern Australia. *Contrib. Mineral. Petrol.* **1982**, *80*, 189–200. [CrossRef]
105. Dawei, H.; Shiguang, W.; Baofu, H.; Manyuan, J. Post-orogenic alkaline granites from China and comparisons with anorogenic alkaline granites elsewhere. *J. Southeast Asian Earth Sci.* **1996**, *13*, 13–27. [CrossRef]

106. El-Bialy, M.Z.; Streck, M.J. Late Neoproterozoic alkaline magmatism in the Arabian–Nubian Shield: The postcollisional A-type granite of Sahara–Umm Adawi pluton, Sinai, Egypt. *Arab. J. Geosci.* **2009**, *2*, 151–174. [CrossRef]
107. Abdel-Rahman, A.-F.M.; El-Kibbi, M.M. Anorogenic magmatism: Chemical evolution of the Mount El-Sibai A-type complex (Egypt), and implications for the origin of within-plate felsic magmas. *Geol. Mag.* **2001**, *138*, 67–85. [CrossRef]
108. Sylvester, P.J. Post-collisional alkaline granites. *J. Geol.* **1989**, *97*, 261–280. [CrossRef]
109. Bonin, B. From orogenic to anorogenic settings: Evolution of granitoid suites after a major orogenesis. *Geol. J.* **1990**, *25*, 261–270. [CrossRef]
110. De la Roche, H.; Leterrier, J.; Grandclaude, P.; Marchal, M. A classification of volcanic and plutonic rocks using R_1R_2-diagram and major-element analyses—Its relationships with current nomenclature. *Chem. Geol.* **1980**, *29*, 183–210. [CrossRef]
111. Batchelor, R.A.; Bowden, P. Petrogenetic interpretation of granitoid rock series using multicationic parameters. *Chem. Geol.* **1985**, *48*, 43–55. [CrossRef]
112. Pearce, J.A.; Harris, N.B.W.; Tindle, A.G. Trace elements discrimination diagrams for the tectonic interpretation of granitic rocks. *J. Petrol.* **1984**, *25*, 956–983. [CrossRef]
113. Pearce, J.A. Sources and settings of granitic rocks. *Episodes* **1996**, *19*, 120–125. [CrossRef]
114. Harris, N.B.W.; Pearce, J.A.; Tindle, A.G. Geochemical characteristics of collision-zone magmatism. In *Collision Tectonics*; Coward, M.P., Reis, A.S., Eds.; Geological Society: London, UK; Special Publications: London, UK, 1986; Volume 19, pp. 67–81. [CrossRef]
115. Mushikin, A.; Navon, O.; Halicz, L.; Hartmann, G.; Stein, M. The Petrogenesis of A-type Magmas from the Amram Massif, Southern Israel. *J. Petrol.* **2003**, *44*, 815–832. [CrossRef]
116. Clemens, J.D.; Holloway, J.R.; White, A.J.R. Origin of an A-type granite: Experimental constraints. *Am. Mineral.* **1986**, *71*, 317–324.
117. Creaser, R.A.; Price, R.C.; Wormald, R.J. A-type granites revisited: Assessment of a residual-source model. *Geology* **1991**, *19*, 163–166. [CrossRef]
118. Patino Douce, A.E.; Beard, J.S. Dehydration melting of biotite gneiss and quartz amphibolite from 3 to 15 kbar. *J. Petrol.* **1995**, *36*, 707–738. [CrossRef]
119. Landenberger, B.; Collins, W.J. Derivation of A-Type Granites from a Dehydrated Charnockitic Lower Crust: Evidence from the Chaelundi Complex, Eastern Australia. *J. Petrol.* **1996**, *37*, 145–170. [CrossRef]
120. Patino Douce, A.E. Generation of metaluminous A-type granites by low-pressure melting of calc-alkaline granitoids. *Geology* **1997**, *25*, 743–746. [CrossRef]
121. Foland, K.A.; Allen, J.C. Magma sources for Mesozoic anorogenic granites of the White Mountain magma series, New England, USA. *Contrib. Mineral. Petrol.* **1991**, *109*, 195–211. [CrossRef]
122. Mingram, B.; Trumbull, R.B.; Littman, S.; Gerstenberger, H. A petrogenetic study of anorogenic felsic magmatism in the Cretaceous Paresis ring complex, Namibia: Evidence for mixing of crust and mantle-derived components. *Lithos* **2000**, *54*, 1–22. [CrossRef]
123. Wu, F.; Sun, D.; Li, H.; Jahn, B.; Wilde, S. A-type granites in northeastern China: Age and geochemical constraints on their petrogenesis. *Chem. Geol.* **2002**, *187*, 143–173. [CrossRef]
124. Yang, J.-H.; Wu, F.-Y.; Chung, S.-L.; Wilde, S.A.; Chu, M.-F. A hybrid origin for the Qianshan A-type granite, northeast China: Geochemical and Sr–Nd–Hf isotopic evidence. *Lithos* **2006**, *89*, 89–106. [CrossRef]
125. Dall'Agnol, R.; de Oliveira, D.C. Oxidized, Magnetite-Series, Rapakivi-Type Granites of Carajás, Brazil: Implications for Classification and Petrogenesis of A-Type Granites. *Lithos* **2007**, *93*, 215–233. [CrossRef]
126. Rämö, O.T.; Haapala, I. One hundred years of rapakivi granite. *Miner. Petrol.* **1995**, *52*, 129–185. [CrossRef]
127. Boztuğ, D.; Harlavan, Y.; Arehart, G.B.; Satir, M.; Avci, N. K–Ar age, whole-rock and isotope geochemistry of A-type granitoids in the Divriği-Sivas region, eastern-central Anatolia, Turkey. *Lithos* **2007**, *97*, 193–218. [CrossRef]
128. Konopelko, D.; Biske, G.; Seltmann, R.; Eklund, O.; Belyatsky, B. Hercynian post-collisional A-type granites of the Kokshaal Range, Southern Tien Shan, Kyrgyzstan. *Lithos* **2007**, *97*, 140–160. [CrossRef]
129. Peng, T.; Wilde, S.A.; Wang, Y.; Fan, W.; Peng, B. Mid-Triassic felsic igneous rocks from the southern Lancangjiang Zone, SW China: Petrogenesis and implications for the evolution of Paleo-Tethys. *Lithos* **2013**, *168–169*, 15–32. [CrossRef]
130. Kang, L.; Xiao, P.-X.; Gao, X.-F.; Xi, R.-G.; Yang, Z.-C. Age, petrogenesis and tectonic implications of Early Devonian bimodal volcanic rocks in the South Altyn, NW China. *J. Asian Earth Sci.* **2015**, *111*, 733–750. [CrossRef]
131. Rudnick, R.L.; Gao, S. The Composition of the Continental Crust. In *Treatise on Geochemistry*; Holland, H.D., Turekian, K.K., Eds.; Elsevier-Pergamon: Oxford, UK, 2003; Volume 3, pp. 1–64. [CrossRef]
132. Moreno, J.A.; Molina, J.F.; Montero, P.; Abu Anbar, M.; Scarrow, J.H.; Cambeses, A.; Bea, F. Unraveling sources of A-type magmas in juvenile continental crust: Constraints from compositionally diverse Ediacaran post-collisional granitoids in the Katerina Ring Complex, southern Sinai, Egypt. *Lithos* **2014**, *192–195*, 56–85. [CrossRef]
133. Moreno, J.A.; Molina, J.F.; Bea, F.; Abu Anbar, M.; Monteroa, P. Th-REE- and Nb-Ta-accessory minerals in post-collisional Ediacaran felsic rocks from the Katerina Ring Complex (S. Sinai, Egypt): An assessment for the fractionation of Y/Nb, Th/Nb, La/Nb and Ce/Pb in highly evolved A-type granites. *Lithos* **2016**, *258–259*, 173–196. [CrossRef]
134. McDonough, W.F.; Sun, S.-S. The composition of the Earth. *Chem. Geol.* **1995**, *120*, 223–253. [CrossRef]

135. Taylor, S.R.; McLennan, S.M. *The Continental Crust: Its Composition and Evolution*; Blackwell Scientific Publications: Oxford, UK, 1985; 312p. [CrossRef]
136. Rudnick, R.L.; Fountain, D.M. Nature and composition of the continental crust: A lower crustal perspective. *Rev. Geophys.* **1995**, *33*, 267–309. [CrossRef]
137. Wedepohl, K.H. The composition of the continental crust. *Geochim. Cosmochim. Acta* **1995**, *59*, 1217–1232. [CrossRef]
138. Chazot, G.; Bertrand, H. Genesis of silicic magmas during tertiary continental rifting in Yemen. *Lithos* **1995**, *36*, 69–83. [CrossRef]
139. Anderson, J.L. Proterozoic anorogenic granite plutonism of North America. In *Proterozoic Geology: Selected Papers from an International Proterozoic Symposium*; Medaris, L.G., Mickelson, D.M., Byers, C.W., Shanks, W.C., Eds.; Geological Society of America Memoir; Geological Society of America: Boulder, CO, USA, 1983; Volume 161, pp. 133–154.
140. Skjerlie, K.P.; Patino Douce, A.E.; Johnston, A.D. Fluid absent melting of a layered crustal protolith: Implications for the generation of anatectic granites. *Contrib. Mineral. Petrol.* **1993**, *114*, 365–378. [CrossRef]
141. Patiño Douce, A.E. What do experiments tell us about the relative contributions of crust and mantle to the origin of granitic magmas? *Geol. Soc. Lond. Spec. Publ.* **1999**, *168*, 55–75. [CrossRef]
142. Koester, E.; Pawley, A.R.; Fernandes, L.A.D.; Pocher, C.C.; Soliani, E., Jr. Experimental Melting of Cordierite Gneiss and the Petrogenesis of Syntranscurrent Peraluminous Granites in Southern Brazil. *J. Petrol.* **2002**, *43*, 1595–1616. [CrossRef]
143. Eyal, M.; Litvinovsky, B.A.; Katzir, Y.; Zanvilevich, A.N. The Pan-African high-K calc-alkaline peraluminous Elat granite from southern Israel: Geology, geochemistry and petrogenesis. *J. Afr. Earth Sci.* **2004**, *40*, 115–136. [CrossRef]
144. Anderson, J.L.; Morrison, J. Ilmenite, magnetite, and peraluminous Mesoproterozoic anorogenic granites of Laurentia and Baltica. *Lithos* **2005**, *80*, 45–60. [CrossRef]
145. Villaseca, C.; Pérez-Soba, C.; Merino, E.M.; Orejana, D.; López-García, J.A.; Billstrom, K. Contrasted crustal sources for peraluminous granites of the segmented Montes de Toledo Batholith (Iberian Variscan Belt). *J. Geosci.* **2008**, *53*, 263–280. [CrossRef]
146. Mao, J.; Takahashi, Y.; Kee, W.-S.; Li, Z.; Ye, H.; Zhao, X.; Liu, K.; Zhou, J. Characteristics and geodynamic evolution of Indosinian magmatism in South China: A case study of the Guikeng pluton. *Lithos* **2011**, *127*, 535–551. [CrossRef]
147. Huang, H.-Q.; Li, X.-H.; Li, W.-X.; Li, Z.-X. Formation of high $\delta^{18}O$ fayalite-bearing A-type granite by high-temperature melting of granulitic metasedimentary rocks, southern China. *Geology* **2011**, *39*, 903–906. [CrossRef]
148. Vielzeuf, D.; Holloway, J.R. Experimental determination of the fluid-absent melting relations in the pelitic system. Consequences for crustal differentiation. *Contrib. Mineral. Petrol.* **1988**, *98*, 257–276. [CrossRef]
149. Patiño Douce, A.E.; Johnston, A.D. Phase equilibria and melt productivity in the pelitic system: Implications for the origin of peraluminous granitoids and aluminous granulites. *Contrib. Mineral. Petrol.* **1991**, *107*, 202–218. [CrossRef]
150. Patiño Douce, A.E.; Beard, J.S. Effects of P, f(O_2) and Mg/Fe ratio on dehydration melting of model metagreywackes. *J. Petrol.* **1996**, *37*, 999–1024. [CrossRef]
151. Patiño Douce, A.E.; McCarthy, T.C. Melting of crustal rocks during continental collision and subduction. In *When Continents Collide: Geodynamics and Geochemistry of Ultrahigh-Pressure Rocks*; Hacker, B.R., Liou, J.G., Eds.; Petrology and Structural Geology; Springer: Dordrecht, The Netherlands, 1998; Volume 10, pp. 27–55. [CrossRef]
152. Altherr, R.; Holl, A.; Hegner, E.; Langer, C.; Kreuzer, H. High potassium, calc-alkaline I-type plutonism in the European Variscides: Northern Vosges (France) and northern Schwarzwald (Germany). *Lithos* **2000**, *50*, 51–73. [CrossRef]
153. Harris, N.B.W.; Inger, S. Trace element modelling of pelite-derived granites. *Contrib. Mineral. Petrol.* **1992**, *110*, 46–56. [CrossRef]
154. Condie, K.C. Chemical composition and evolution of the upper continental crust: Contrasting results from surface samples and shales. *Chem. Geol.* **1993**, *104*, 1–37. [CrossRef]
155. Skjerlie, K.P.; Johnston, A.D. Vapour-Absent Melting from 10 to 20 kbar of Crustal Rocks that Contain Multiple Hydrous Phases: Implications for Anatexis in the Deep to Very Deep Continental Crust and Active Continental Margins. *J. Petrol.* **1996**, *37*, 661–691. [CrossRef]
156. Jung, S.; Pfänder, J.A. Source composition and melting temperatures of orogenic granitoids: Constraints from CaO/Na_2O, Al_2O_3/TiO_2 and accessory mineral saturation thermometry. *Eur. J. Mineral.* **2007**, *19*, 859–870. [CrossRef]
157. Clemens, J.D.; Wall, V.J. Origin and crystallization of some peraluminous (S-type) granitic magmas. *Can. Mineral.* **1981**, *19*, 111–131.
158. Watson, E.B.; Harrison, T.M. Zircon saturation revisited: Temperature and composition effects in a variety of crustal magma types. *Earth Planet Sci. Lett.* **1983**, *64*, 295–304. [CrossRef]
159. Miller, C.F.; McDowell, S.M.; Mapes, R.W. Hot and cold granites? Implications of zircon saturation temperatures and preservation of inheritance. *Geology* **2003**, *31*, 529–532. [CrossRef]
160. Bucholz, C.E.; Spencer, C.J. Strongly Peraluminous Granites across the Archean–Proterozoic Transition. *J. Petrol.* **2019**, *60*, 1299–1348. [CrossRef]
161. Watson, E.B.; Harrison, T.M. Accessory minerals and the geochemical evolution of crustal magmatic systems: A summary and prospectus of experimental approaches. *Phys. Earth Planet. Inter.* **1984**, *35*, 19–30. [CrossRef]

162. King, P.L.; Chappell, B.W.; Allen, C.M.; White, A.J.R. Are A-type granites the high-temperature felsic granites? Evidence from fractionated granites of the Wangrah Suite. *Aust. J. Earth Sci.* **2001**, *48*, 501–514. [CrossRef]
163. Watt, G.R.; Harley, S.L. Accessory phase controls on the geochemistry of crustal melts and restites produced during water undersaturated partial melting. *Contrib. Mineral. Petrol.* **1993**, *101*, 220–231. [CrossRef]
164. Beard, J.S.; Lofgren, G.E.; Sinha, K.; Tollo, R.P. Partial melting of apatite-bearing charnockite, granulite, and diorite: Melt compositions, restite mineralogy, and petrologic implications. *J. Geophys. Res.* **1994**, *99*, 21591–21603. [CrossRef]
165. Ayres, M.; Harris, N. REE fractionation and Nd-isotope disequilibrium during crustal anatexis: Constraints from Himalayan leucogranites. *Chem. Geol.* **1997**, *139*, 249–269. [CrossRef]
166. Peccerillo, A.; Barberio, M.R.; Yirgu, G.; Ayalew, D.; Barbieri, M.; Wu, T.W. Relationships between Mafic and Peralkaline Silicic Magmatism in Continental Rift Settings: A Petrological, Geochemical and Isotopic Study of the Gedemsa Volcano, Central Ethiopian Rift. *J. Petrol.* **2003**, *44*, 2003–2032. [CrossRef]
167. Condie, K.C. Archean magmatism and crustal thickening. *Geol. Soc. Am. Bull.* **1973**, *84*, 2981–2992. [CrossRef]
168. Conrad, W.K.; Nicholls, I.A.; Wall, V.J. Water-Saturated and -Undersaturated Melting of Metaluminous and Peraluminous Crustal Compositions at 10 kb: Evidence for the Origin of Silicic Magmas in the Taupo Volcanic Zone, New Zealand, and Other Occurrences. *J. Petrol.* **1988**, *29*, 765–803. [CrossRef]
169. Singh, J.; Johannes, W. Dehydration Melting of Tonalites. Part I. Beginning of Melting. *Contrib. Mineral. Petrol.* **1996**, *125*, 16–25. [CrossRef]
170. Montel, J.-M.; Vielzeuf, D. Partial melting of metagreywackes, Part II. Compositions of minerals and melts. *Contrib. Mineral. Petrol.* **1997**, *128*, 176–196. [CrossRef]
171. Watkins, J.M.; Clemens, J.D.; Treloar, P.J. Archaean TTGs as sources of younger granitic magmas: Melting of sodic metatonalites at 0.6–1.2 GPa. *Contrib. Mineral. Petrol.* **2007**, *154*, 91–110. [CrossRef]
172. Weinberg, R.F.; Hasalova, P. Water-fluxed melting of the continental crust: A review. *Lithos* **2015**, *212–215*, 158–188. [CrossRef]
173. Gao, P.; Zheng, Y.-F.; Zhao, Z.-F. Experimental melts from crustal rocks: A lithochemical constraint on granite petrogenesis. *Lithos* **2016**, *266–267*, 133–157. [CrossRef]
174. Harris, N.; Inger, S.; Massey, J. The role of fluids in the formation of High Himalayan leucogranites. *Geol. Soc. Spec. Publ.* **1993**, *74*, 391–400. [CrossRef]
175. Patiño Douce, A.E.; Harris, N. Experimental constraints on Himalayan anatexis. *J. Petrol.* **1998**, *39*, 689–710. [CrossRef]
176. Vielzeuf, D.; Schmidt, N.W. Melting relations in hydrous systems revisited: Application to metapelites, metagreywackes and metabasalts. *Contrib. Mineral. Petrol.* **2001**, *141*, 251–267. [CrossRef]
177. Le Breton, N.; Thompson, A.B. Fluid-absent (dehydration) melting of biotite in metapelites in the early stages of crustal anatexis. *Contrib. Mineral. Petrol.* **1988**, *99*, 226–237. [CrossRef]
178. Finger, F.; Schiller, D. Lead contents of S-type granites and their petrogenetic significance. *Contrib. Mineral. Petrol.* **2012**, *164*, 747–755. [CrossRef]
179. Waters, D.J.; Whales, C.J. Dehydration melting and the granulite transition in metapelites from southern Namaqualand, S. Africa. *Contrib. Mineral. Petrol.* **1984**, *88*, 269–275. [CrossRef]
180. Vernon, R.H.; Collins, W.J. Igneous microstructures in migmatites. *Geology* **1988**, *16*, 1126–1129. [CrossRef]
181. Clemens, J.D.; Vielzeuf, D. Constraints on melting and magma production in the crust. *Earth Planet. Sci. Lett.* **1987**, *86*, 287–306. [CrossRef]
182. Vielzeuf, D.; Montel, J.M. Partial melting of metagreywackes. Part I. Fluid-absent experiments and phase relationships. *Contr. Mineral. Petrol.* **1994**, *117*, 375–393. [CrossRef]
183. Johnson, T.E.; White, R.W.; Powell, R. Partial melting of metagreywacke: A calculated mineral equilibria study. *J. Metamorph. Geol.* **2008**, *26*, 837–853. [CrossRef]
184. Wang, Q.; Chung, S.-L.; Li, X.-H.; Wyman, D.; Li, Z.-X.; Sun, W.-D.; Qiu, H.-N.; Liu, Y.-S.; Zhu, Y.-T. Crustal melting and flow beneath northern Tibet: Evidence from mid-miocene to quaternary strongly peraluminous rhyolites in southern Kunlun Range. *J. Petrol.* **2012**, *53*, 2523–2566. [CrossRef]
185. Wang, Q.; Hawkesworth, C.J.; Wyman, D.; Chung, S.-L.; Wu, F.-Y.; Li, X.-H.; Li, Z.-X.; Gou, G.-N.; Zhang, X.-Z.; Tang, G.-J.; et al. Pliocene-Quaternary crustal melting in central and northern Tibet and insights into crustal flow. *Nat. Commun.* **2016**, *7*, 11888. [CrossRef]
186. Dini, A.; Gianelli, G.; Puxeddu, M.; Ruggieri, G. Origin and evolution of Pliocene-Pleistocene granites from the Larderello geothermal field (Tuscan Magmatic Province, Italy). *Lithos* **2005**, *81*, 1–31. [CrossRef]
187. Holtz, F.; Johannes, W.; Tamic, N.; Behrens, H. Maximum and minimum water contents of granitic melts generated in the crust: A revaluation and implications. *Lithos* **2001**, *56*, 1–14. [CrossRef]
188. Castro, A.; Corretgé, L.G.; El-Biad, M.; El-Hmidi, H.; Fernández, C.; Patiño Douce, A.E. Experimental constraints on Hercynian anatexis in the Iberian Massif, Spain. *J. Petrol.* **2000**, *41*, 1471–1488. [CrossRef]

189. Stevens, G.; Clemens, J.D.; Droop, G.T.R. Melt production during granulite-facies anatexis: Experimental data from "primitive" metasedimentary protoliths. *Contrib. Mineral. Petrol.* **1997**, *128*, 352–370. [CrossRef]
190. García-Casco, A.; Haissen, F.; Castro, A.; El-Hmidi, H.; Torres-Roldan, R.L.; Millán, G. Synthesis of staurolite in melting experiments of a natural metapelite: Consequences for the phase relations in low-temperature pelitic migmatites. *J. Petrol.* **2003**, *44*, 1727–1757. [CrossRef]
191. Rapp, R.P.; Watson, E.B. Dehydration melting of metabasalt at 8–32 kbar: Implications for continental growth and crust-mantle recycling. *J. Petrol.* **1995**, *36*, 891–931. [CrossRef]
192. Rapp, R.P.; Shimizu, N.; Norman, M.D. Growth of early continental crust by partial melting of eclogite. *Nature* **2003**, *425*, 605–609. [CrossRef] [PubMed]
193. Patiño Douce, A.E. Vapor-absent melting of tonalite at 15–32 kbar. *J. Petrol.* **2005**, *46*, 275–290. [CrossRef]
194. Hanson, G.N. The application of trace elements to the petrogenesis of igneous rocks of granitic composition. *Earth Plant. Sci. Lett.* **1978**, *39*, 26–34. [CrossRef]
195. Wang, W.; Pandit, M.K.; Zhao, J.-H.; Chen, W.-T.; Zheng, J.-P. Slab break-off triggered lithosphere—Asthenosphere interaction at a convergent margin: The Neoproterozoic bimodal magmatism in NW India. *Lithos* **2018**, *296–299*, 281–296. [CrossRef]
196. Zhao, J.-L.; Qiu, J.-S.; Liu, L.; Wang, R.-Q. The Late Cretaceous I- and A-type granite association of southeast China: Implications for the origin and evolution of post-collisional extensional magmatism. *Lithos* **2016**, *240–243*, 16–33. [CrossRef]
197. Kaur, P.; Zeh, A.; Chaudhri, N.; Eliyas, N. Two distinct sources of 1.73–1.70 Ga A-type granites from the northern Aravalli orogen, NW India: Constraints from in situ zircon U-Pb ages and Lu-Hf isotopes. *Gondwana Res.* **2017**, *49*, 164–181. [CrossRef]
198. Zhao, K.-D.; Liu, G.-Q.; Jiang, S.-Y. Petrogenesis and Tectonic Implications of the Yuhuashan A-Type Volcanic-Intrusive Complex and Mafic Microgranular Enclaves in the Gan-Hang Volcanic Belt, Southeast China. *J. Geol.* **2019**, *127*, 37–59. [CrossRef]
199. Ma, X.; Song, Y.; Tang, J.; Chen, W. Newly identified rhyolite-biotite monzogranite (A2-type granite)-norite belt from the Bangong-Nujiang collision zone in Tibet Plateau: Evidence for the slab break-off beneath the Lhasa Terrane. *Lithos* **2020**, *366–367*, 105565. [CrossRef]
200. Liu, H.-D.; Cheng, Y.-H.; Santosh, M.; Teng, X.-M.; Zhang, X.-W.; Teng, X.-J. Magmatism associated with lithospheric thinning, mantle upwelling, and extensional tectonics: Evidence from Carboniferous-Permian dyke swarms and granitoids from Inner Mongolia, Central Asian Orogenic Belt. *Lithos* **2021**, *386–387*, 106004. [CrossRef]
201. Bonev, N.; Dilek, Y. Geochemistry and tectonic significance of proto-ophiolitic metamafic units from the Serbo-Macedonian and western Rhodope massifs (Bulgaria-Greece). *Int. Geol. Rev.* **2009**, *52*, 298–335. [CrossRef]
202. Vavassis, I.; de Bono, A.; Stampfli, G.M.; Giorgis, D.; Valloton, A.; Amelin, Y. U-Pb and Ar-Ar geochronological data from the Pelagonian basement in Evia (Greece): Geodynamic implications for the evolution of Paleotethys. *Schweiz. Mineral. Petrogr. Mitt.* **2000**, *80*, 21–43.
203. Anders, B.; Reischmann, T.; Kostopoulos, D. Zircon geochronology of the basement rocks from the Pelagonian zone, Greece: Constraints on the pre-Alpine evolution of the westernmost Internal Hellenides. *Int. J. Earth Sci.* **2007**, *96*, 639–661. [CrossRef]
204. Spahić, D.; Gaudenyib, T.; Glavaš-Trbić, B. A hidden suture within the northern Paleotethyan margin: Paleogeographic/paleo-tectonic constraints on the late Paleozoic "Veles series" (Vardar Zone, North Macedonia). *Proc. Geologist. Assoc.* **2019**, *130*, 701–718. [CrossRef]
205. Šoster, A.; Zavašnik, J.; O'Sullivan, P.; Herlec, U.; Potočnik Krajnc, B.; Palinkaš, L.A.; Zupančič, N.; Dolenec, M. Geochemistry of Bashibos-Bajrambos metasedimentary unit, Serbo-Macedonian massif, North Macedonia: Implications for age, provenance and tectonic setting. *Geochemistry* **2020**, *80*, 125664. [CrossRef]